Advances in Physics: X

ISSN: (Print) (Online) Journal homepage: www.tandfonline.com/journals/tapx20

On ultrafast x-ray scattering methods for magnetism

R. Plumley, S. R. Chitturi, C. Peng, T. A. Assefa, N. Burdet, L. Shen, Z. Chen, A. H. Reid, G. L. Dakovski, M. H. Seaberg, F. O'Dowd, S. A. Montoya, H. Chen, A. Okullo, S. Mardanya, S. D. Kevan, P. Fischer, E. E. Fullerton, S. K. Sinha, W. Colocho, A. Lutman, F.-J. Decker, S. Roy, J. Fujioka, Y. Tokura, M. P. Minitti, J. A. Johnson, M. Hoffmann, M. E. Amoo, A. Feiguin, C. Yoon, J. Thayer, Y. Nashed, C. Jia, A. Bansil, S. Chowdhury, A. M. Lindenberg, M. Dunne, E. Blackburn & J. J. Turner

To cite this article: R. Plumley, S. R. Chitturi, C. Peng, T. A. Assefa, N. Burdet, L. Shen, Z. Chen, A. H. Reid, G. L. Dakovski, M. H. Seaberg, F. O'Dowd, S. A. Montoya, H. Chen, A. Okullo, S. Mardanya, S. D. Kevan, P. Fischer, E. E. Fullerton, S. K. Sinha, W. Colocho, A. Lutman, F.-J. Decker, S. Roy, J. Fujioka, Y. Tokura, M. P. Minitti, J. A. Johnson, M. Hoffmann, M. E. Amoo, A. Feiguin, C. Yoon, J. Thayer, Y. Nashed, C. Jia, A. Bansil, S. Chowdhury, A. M. Lindenberg, M. Dunne, E. Blackburn & J. J. Turner (2024) On ultrafast x-ray scattering methods for magnetism, Advances in Physics: X, 9:1, 2423935, DOI: 10.1080/23746149.2024.2423935

To link to this article: https://doi.org/10.1080/23746149.2024.2423935

Published online: 24 Nov 2024.

ADVANCES IN PHYSICS: X
2024, VOL. 9, NO. 01, 1–39
https://doi.org/10.1080/23746149.2024.2423935

Taylor & Francis
Taylor & Francis Group

REVIEWS

On ultrafast x-ray scattering methods for magnetism

R. Plumley, S. R. Chitturi, C. Peng, T. A. Assefa, N. Burdet, L. Shen, Z. Chen, A. H. Reid, G. L. Dakovski, M. H. Seaberg, F. O'Dowd, S. A. Montoya, H. Chen, A. Okullo, S. Mardanya, S. D. Kevan, P. Fischer, E. E. Fullerton, S. K. Sinha, W. Colocho, A. Lutman, F.-J. Decker, S. Roy, J. Fujioka, Y. Tokura, M. P. Minitti, J. A. Johnson, M. Hoffmann, M. E. Amoo, A. Feiguin, C. Yoon, J. Thayer, Y. Nashed, C. Jia, A. Bansil, S. Chowdhury, A. M. Lindenberg, M. Dunne, E. Blackburn and J. J. Turner

[a]Stanford Institute for Materials and Energy Sciences, Stanford University and SLAC National Accelerator Laboratory, Menlo Park, CA, USA; [b]Linac Coherent Light Source, SLAC National Accelerator Laboratory, Menlo Park, CA, USA; [c]Department of Physics and Astronomy, Carnegie Mellon University, Pittsburgh, PA, USA; [d]Department of Materials Science and Engineering, Stanford University, Stanford, CA, USA; [e]Division of Synchrotron Radiation Research, Department of Physics, Lund University, Lund, Sweden; [f]Center for Memory and Recording Research, University of California–San Diego, La Jolla, CA, USA; [g]Physics Department, Northeastern University, Boston, MA, USA; [h]Department of Physics and Astronomy, Howard University, Washington, DC, USA; [i]Department of Physics, University of Oregon, Eugene, OR, USA; [j]Advanced Light Source, Lawrence Berkeley National Laboratory, Berkeley, CA, USA; [k]Materials Sciences Division, Lawrence Berkeley National Laboratory, Berkeley, CA, USA; [l]Department of Electrical and Computer Engineering, University of California–San Diego, La Jolla, CA, USA; [m]Department of Physics, University of California–San Diego, La Jolla, CA, USA; [n]Department of Applied Physics and Quantum-Phase Electronics Center, University of Tokyo, Hongo, Tokyo, Japan; [o]Graduate School of Pure and Applied Sciences, University of Tsukuba, Tsukuba, Ibaraki, Japan; [p]Center for Emergent Matter Science, RIKEN Center for Emergent Matter Science (CEMS), Wako, Japan; [q]Swiss Light Source, Paul Scherrer Institut, Villigen-PSI, Switzerland; [r]Department of Mechanical Engineering, Howard University, Washington, DC, USA and [s]Machine Learning Department, SLAC National Accelerator Laboratory, Menlo Park, CA, USA

ABSTRACT

With the introduction of x-ray free electron laser sources around the world, new scientific approaches for visualizing matter at fundamental length and time-scales have become possible. As it relates to magnetism and 'magnetic-type' systems, advanced scattering methods are being developed for studying ultrafast magnetic responses on the time-scales at which they occur. We describe three capabilities which have the potential to seed new directions in this area and present

ARTICLE HISTORY
Received 28 July 2023
Accepted 25 October 2024

KEYWORDS
Ultrafast; x-rays; magnetism; x-ray free electron lasers; machine-learning; instrumentation

CONTACT S. Chowdhury sugata.chowdhury@howard.edu Department of Physics and Astronomy, Howard University, Washington, DC 94025, USA; A. M. Lindenberg aaronl@stanford.edu Department of Materials Science & Engineering, Stanford University, Stanford, CA 94305, USA; J. J. Turner joshuat@stanford.edu Stanford Institute for Materials & Energy Sciences, Stanford University and SLAC National Accelerator Laboratory, Menlo Park, CA 20059, USA

original results from each: pump-probe x-ray scattering with low energy excitation, x-ray photon fluctuation spectroscopy, and ultrafast diffuse x-ray scattering. By combining these experimental techniques with advanced modeling together with machine learning, we describe how the combination of these domains allows for a new understanding in the field of magnetism. Finally, we give an outlook for future areas of investigation and the newly developed instruments which will take us there.

GRAPHICAL ABSTRACT

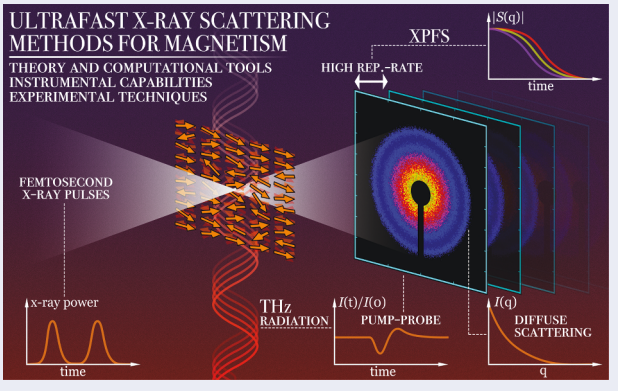

1 Introduction

In recent years, remarkable new phases of matter have been both predicted and measured, such as quantum spin liquids, skyrmions, strongly spin-orbit coupled materials, quantum spin Hall insulators, and helical topological superconductors [1]. These phases often arise due to delicate combinations of multiple interactions such as quantum confinement or magnetic frustration, and can display magnetic features with both short-range and long-range order from sub-nanometer to micron length scales [2]. Quantum materials exhibiting this behavior hold promise for highly efficient electronic- and spin-transport as well as tunability for technological applications [3,4]. One such field is that of spintronics, where the magnetic degree of freedom can be used as a knob for new functionalities and enable new abilities to control materials [5,6]. For instance, controlling the anisotropy can be accomplished by field tuning a spin- 1/2 system to transform an isotropic 2D Heisenberg to the highly anisotropic 2D XY system [7].

A common theme in 'quantum engineering' of materials and devices is the ability to temporarily drive one phase into another, usually by the introduction of a symmetry-breaking mechanism or radiative excitation [8–14], or to create new transient states of matter [15–17]. This necessitates a robust theoretical understanding of how systems respond to stimulation at ultrafast time-scales. One such example in the field of magnetism is the 2D van der Waals materials [18,19]. Here, theoretical models can be tested directly,

such as the Berezinskii-Kosterlitz-Thouless transition which predicts topological order. In the 2D limit, magnetic fluctuations can become dominant, and can also act to mediate the formation of other types of hidden quantum phases [20]. Probing such fluctuations requires the development of new experimental tools with sensitivity on the requisite time- and length- scales.

Another rapidly growing field of study is the understanding and control of discrete topological objects, such as magnetic skyrmions. These have been shown to respond to small magnetic fields with incredible implications for technological applications such as computer memory [3,21]. While the motion of individual spin-moments can be described on the nanosecond timescale by the Landau-Lifshitz-Gilbert equation, descriptions of spin-dynamics alone are insufficient for getting the full picture, since the emergence of skyrmion spin-textures arise from complicated competitions between a host of magnetic interactions, and can involve quasi-particles which are many lattice units in size. These structures exhibit dynamics that range across many time-scales from microseconds to the ultrafast, and can span length-scales much larger than the unit cells of their parent lattice [10,22–24].

Many powerful scattering methods exist and have continued to be developed for understanding dynamics related to novel magnetic phenomena. This is commonly explored through inelastic spectroscopy techniques, such as static and time-resolved resonant inelastic x-ray scattering. This is a superb option to measure magnetic excitations that has been successful on a number of systems and has shown a lot of potential [25–29], but is quite far from the caliber of energy resolution delivered by neutrons. Small-angle neutron scattering (SANS) as well as inelastic neutron scattering have also been used profitably to study complex magnetic textures [30,31]. In neutron spin-echo spectroscopy (NSE) [32,33] the dynamic structure factor can be accessed down to nanosecond time-scales with atomic precision, but can sometimes be challenging compared to x-ray sources due to the low scattering cross-section and absorption of neutrons in some materials, as compared x-rays. This aspect can hinder the capability of neutron methods for studying thin samples and systems undergoing rapid time-development, because the neutron signal flux has to be averaged over long times. In order to make continued progress, novel methods are needed to access magnetic structure and excitations at relevant length-scales as above, but that additionally can access dynamic phenomena at ultrafast timescales.

Complementary tools now are available which can target some of the modern topics in magnetism for the study of dynamics at the atomic scale using X-ray Free-Electron Lasers (X-FEL). This effort has a long history [34], from the first demonstrated rapid quenching of magnetic order [35] to the early use case of using the Stanford Linear Accelerator to create short magnetic field pulses to read and write in magnetic recording media [36] Currently these new machines are creating enhanced capabilities in this area (for some

good reviews, see [37–39]). These types of sources have had impact in many scientific research areas [40], notably in wide-ranging areas such as atomic and molecular science [41–43], astrophysics [44,45], condensed matter and materials physics [15,46–48], and structural biology [49,50]. This versatility is mainly owing to the ability to provide femtosecond x-ray pulse durations, large pulse energies, and repetition rates, up to theorder of a MHz [40,51–53]. The photon energy is also typically tunable, allowing for element-specific resonant x-ray scattering for instance, which can isolate and enhance the magnetic structure signal from the sample [54–60]. These next generation light sources hold vast potential for driving the field of magnetism to new heights.

It is in this context that we provide a forward-looking perspective in the field of magnetism focused on methods based on X-FEL radiation, especially as it relates to the ultrafast regime. We specifically focus on three methods which could be transformative in this area. With a close coupling between theory, combined with recent machine-assisted analysis techniques, we outline recent progress which has occurred by optimizing this overlap. In addition to a description of the experimental methods, we review the theoretical result for the cross-section of magnetic systems to showcase research in this area and to help create an intuitive picture of what each method seeks to measure. We support this with theoretical tools, which have demonstrated potential for advanced time domain studies. These provide theoretical predictions, aiding in the interpretation of phenomena, and offer independent justification for significant progress. Interwoven though all this are new machine learning (ML) advancements which can enhance and accelerate ultrafast materials studies in magnetism. Though there is much progress in the ML field, we choose three 'hot' topics to review for the researchers in ultrafast magnetism that might be new to this area. Finally, we provide an outlook for spin-sensitive studies in the ultrafast regime. We conclude with a discussion on the scientific prospects which will be available with the latest accelerator modes and new instruments being constructed at the LCLS-II.

2 Ultrafast experimental methods

Here we discuss three methods of experimental investigation that can be implemented for studies in ultrafast magnetism at next-generation light sources. The range of examples was chosen to demonstrate the variety of areas in magnetism that can be tackled with X-FELs, which are also linked together with new instrumentation we discuss in Section 5.3. These are quantum materials with strong electron correlation containing low-energy modes – such as those that can be accessed with THz radiation, exotic or textured magnetic phases – such as topological solitons, as well as systems where magnetic frustration plays a deterministic role – for example, Ising spin chains, spin-ices, and spin-glass systems. We outline the three modes of investigation below.

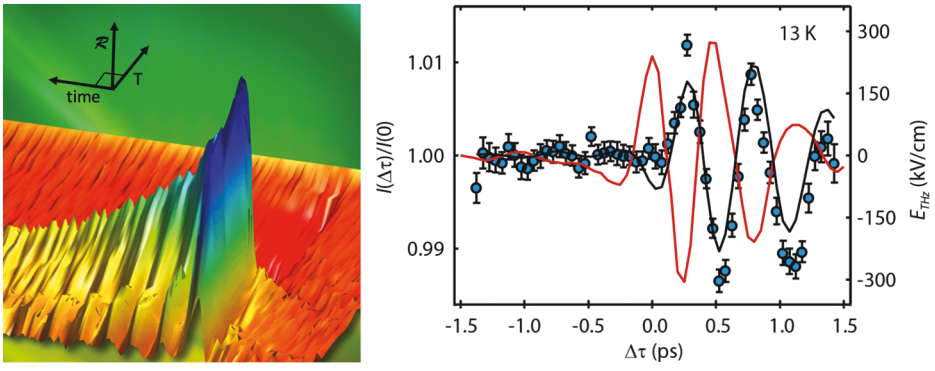

Figure 1. THz excitation in materials. (a) The optical reflectivity at a wavelength of 800 nm showing the rich information available at ultrafast timescales under long wavelength excitation. The system is the high-temperature superconductor $YBa_2Cu_3O_{6+x}$, and was pumped with a strong-field THz excitation of ~400 V/cm and is plotted as a function of both time and temperature (data based on Dakovski and co-workers [62]). (b) The soft x-ray scattering response (blue markers, left axis) in the multiferroic $TbMnO_3$ after THz excitation (red line, right axis) in resonance with an electromagnon. The sub-picosecond pulse can be used to control spin dynamics by inducing the rotation of a spin-cycloid structure in the material [46].

2.1 Thz / X-ray pump-probe scattering

One area of focus combines femtosecond x-ray probes with THz excitation of materials, especially in the area of magnetism [61]. This can provide long wavelength combined with strong electric field excitation to resonantly pump or induce new phenomena in materials, such as the probing of the superconducting condensate (Figure 1a). Using resonant x-ray scattering, the magnetic structure can be directly probed, such as the *L*–edge, responsible for *p*-to-*d* transitions of the magnetic ion. A powerful use of X-FELs is to combine this sensitivity of the magnetic structure with THz excitation. With short-pulsed THz radiation, low energy modes can be directly excited for spin relaxation, spin enhancement, or coherent spin control [46]. For instance, ultrashort THz pump pulses can directly couple to electromagnons (see Figure 2b). By using soft x-ray scattering at the Mn *L*–edge to probe the spin state in $TbMnO_3$, strong field THz was used to both excite and study the response of an electromagnon excitation [63,64]. With current developments underway at the LCLS-II (see Sec.5.3.1 and Sec.5.3.2), THz pumping will soon be possible while probing with high-repetition rate soft x-rays for direct sensitivity to different types of electronic ordering.

Another example is in non-resonant THz pumping, where THz excitation has been shown to have spin sensitivity. Preliminary measurements were carried out [65] on a manganite single crystal of $Nd_{1-x}Sr_{1+x}MnO_4$ ($x = 2/3$) consisting of non-resonant THz pumping the system, and x-ray or optical probe. The experimental details are outlined in Appendix 5.4. The main

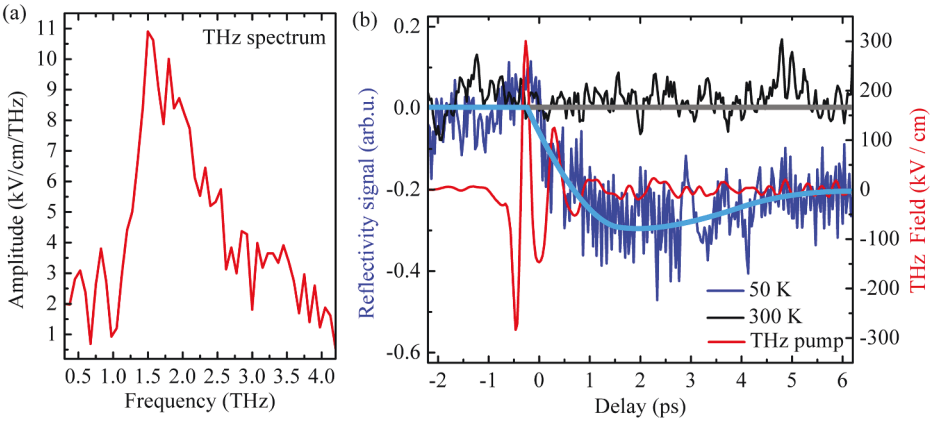

Figure 2. Amplitude spectrum of the THz pump pulse obtained from the Fourier transform of its time trace. (b) Temporal evolution of the 800 nm optical reflectivity (left axis) at 50 K (blue) and 300 K (black) after p-polarized THz photoexcitation of the manganite single crystal, $Nd_{1-x}Sr_{1+x}MnO_4$ ($x = 2/3$). The lower temperature is below the Neel temperature in this crystal and is likely demonstrating enhanced sensitivity to the magnetic order. The time trace of a single THz pulse is shown in red (right axis).

results show THz generation produced through non-linear rectification using a organic crystal to generate high electric field strengths (Figure 2a) and demonstrate how sensitive the magnetic ordering is to THz excitation (Figure 2b). This illustrates the reflectivity response to high-field, short-pulse THz radiation centered at around 1.5 THz, the frequency spectrum of which is shown in Figure 2b. The curves show the THz pulse trace (red), the negligible response to IR light above the ordering temperature at 300K (black), and the response of the spin state which occurs below the Néel temperature (blue). When the crystal is magnetically ordered, the THz response shows a much more dramatic response compared to above room temperature. This is reminiscent of other effects that seem to be enhanced with THz radiation, such as the surprising sensitivity to the superconducting condensate in the presence of charge rather than magnetic order, in the high-temperature superconductor $YBa_2Cu_3O_{6+\delta}$ [62]. These results point to the value of exploiting the use of the strong THz response to magnetic systems with different types of ordering while using the high repetition rate capability at X-FELs to map out the ultrafast magnetic response in fresh detail.

2.2 X-ray photon fluctuation spectroscopy

Another area of anticipation is in using x-ray pulses with different separation times between pulses, to perform 'probe-probe' measurements to study magnetic fluctuations, sometimes referred to as x-ray photon fluctuation spectroscopy' (XPFS) [66]. This is similar to x-ray intensity fluctuation spectroscopy (XIFS) [67] or -ray photon correlation spectroscopy (XPCS) [68],

but instead of correlating scattered x-ray speckle patterns between shots, the shots are added together and the contrast is extracted from the pulse pair, when the pulses within each pair are finely spaced in time. These methods take advantage of the high degree of coherence of the x-rays delivered by advanced light sources to produce 'speckle' patterns, where scattered photons create a complex intensity pattern based on the exact configuration of the system. The given configuration is typically not detected but averaged over when the degree of coherence is not high. By monitoring this speckle pattern, fluctuations of the structure can be measured and related back to theory to directly access the interactions between constituents within the system.

XPFS is an ultrafast version of XIFS or XPCS and is in the spirit of x-ray speckle visibility spectroscopy, where the contrast is analyzed rather than the intensity-intensity autocorrelation function [69,70], but the contrast is obtained from a pair of summed pulses [71]. This benefit provides technical motivation because in this case, the area detector collecting images does not have to be read out at the rate of the pulse separation, but rather the repetition rate of the delivery of pulse pairs from the light source. This capability provides an incredible potential for access to much shorter times. Importantly, the information can still be captured with the summation of the individual pulses, when keeping track of the number of pulses added and with the caveat that the signal-to-noise goes down for multi-shot images.

Furthermore, effects that have long caused major challenges in XPCS, such as beamline vibration, are not cause for concern in this modality. Since this type of measurement consists of comparing a pair of pulses on a much shorter timescale than that of mechanical instabilities, the benefit is that stability of optics or long term drift does not come into play. Additional methods can be implemented as well, such as a contrast monitor [72] consisting of a disordered system like nanoporous glass, which provides a diagnostic of the beam parameters via a high-contrast static speckle pattern that can be used to separate the coherent scattering from the sample. Another strategy is to normalize the two-pulse contrast with the single-shot as an additional frame of reference to separate out sample dynamics as has been shown previously [73]. The pointing of the two beams can also cause concern such as when two beams are split by optical elements to create two paths with different trajectories [74], but under accelerator-based pulse pair conditions, each beam can be finely controlled to travel on the same trajectory and to illuminate the same area of the sample.

By using XPFS, the ground state fluctuations of a magnetic texture in its natural state can be studied, without inducing the non-equilibrium nature which is typically associated with ultrafast methods. This also requires ultrashort pulses to take snapshots of the magnetic state at different times, but the focus is to make a time-resolved comparison of the system under different conditions. For instance, in the multilayered magnetic system FeGd,

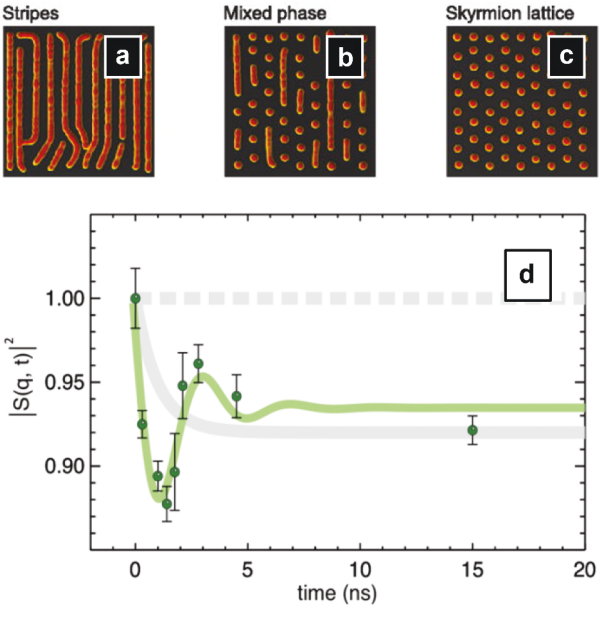

Figure 3. Skyrmion fluctuations. (a-c) In the thin film magnet FeGd, the ferromagnetic stripe phase transforms to a skrymion lattice state by what seems to be a mixed phase [73]. Black and orange represent opposite, out-of-plane spin directions, where the more complicated 'vortex-like' spin texture within each individual skyrmion is not shown here. (d) The time-dependent structure factor $S(\mathbf{q}, t)$ of the skyrmion lattice of FeGd recorded at the skyrmion lattice scattering peak [75]. This multi-layered system forms a skyrmion lattice on the length scale of up to 100 lattice spacings and spontaneous dynamics can be measured with XPFS of this structure on nanosecond times.

the ferromagnetic stripe phase transforms to a skrymion lattice phase (see Figure 3a–c), which has been detected with many techniques [76–78]. Here XPFS has been carried out in both the mixed phase as well as the in the skymrion lattice phase [72,73,75,79]. By varying the pulse separation, a damped 'phonon-like' mode was measured of the skyrmion lattice at the nanosecond timescale [75], due to the large-scale size of the skyrmion structures, of order 100 lattice spacings (see Figure 3d). This is reminiscent of the Goldstone mode seen by neutron spin echo in bulk MnSi [33, 80], but was observed in this skyrmion material by directly probing the resonant scattering from the Gd spins of the magnetic quasi-particles.

A first study has been carried out to follow-up on this work with the new instruments being developed at LCLS-II, with the experimental details described in Appendix 5.5. In this case, a particular set-up was designed to be inserted into the newly developed chemRIXS endstation, which is dedicated to host a liquid chemistry environment, in order to accomodate solid samples for early commissioning. This special setup was based on a prototype of the upcoming XPFS instrumentthe an earlier version of this, the XPFS prototype instrument [72], and is discussed further in Section 5.3.2. However, one issue with this modality is the use of a small area detector which has to be translated

in space to find the necessary scattering. This makes it a formidable challenge to identify what phase the sample is in. By live-scanning the detector over large regions of reciprocal space, we were able to register sub-diffraction images to each other. The first result of this final, stitched diffraction pattern from the detector in this mode is presented in Figure A1 in the Appendix 5.6 where the stripe-skrymion phase was identified. More thorough studies of the fluctuation spectra in this system are on-going.

Moreover, recent work has focused on changing the ratio of the two probes to increase the first well beyond the second pulse by adjusting the pulse energies generated from the machine (Sec. 5.2.1). The idea of this option is to perform x-ray pump / x-ray probe by selectively x-ray pumping the system to study the response with soft x-rays. This is quite different in nature to XPFS and instead has the goal of exciting the system at very high energies.

Finally, we point out the natural extension of this, where one combines XPFS-type measurements with an optical/THz pump pulse to probe non-equilibrium fluctuations in the excited state. Here, the idea would instead be to not keep the system in equilibrium, but to understand how the dynamical heterogeneity takes place during the excitation process, as has been shown in topological-polar materials [81]. This is more sophisticated then a typical pump-probe study because much more information about the length-scale is available than in the scattered intensity. In other words, the monitoring of the contrast can be used for going beyond the coherent response to probe disorder and heterogeneity in non-equilibrium systems as well.

2.3 Ultrafast diffuse X-ray scattering

A third method that will be critical to exploit in the field of ultrafast magnetism is in the study of magnetic disorder or frustration, and is typically studied through diffuse magnetic scattering. Many materials exhibit a well-defined structure with characteristic collective excitations, which can be resolved in reciprocal space and can even be controlled externally (see Sec. 2.1). However, sometimes considerable information is contained away from the well-defined structural responses of the system, in the shorter range interactions, which disturb the density-density correlations and lead to diffuse scattering. This diffuse scattering is typically, but not always, found near the peaks corresponding to the long-range order. For example, just as the thermal motion of atoms about their sites generates thermal diffuse scattering that can be used to obtain information about phonons [82,83], there is analogous diffuse magnetic scattering which can shed light on the magnetic structure as well [84,85] (see Figure 4a,b). Here, magnetic correlations in Weyl semimetals were measured through resonant elastic x-ray scattering. The diffuse scattering provides evidence of ferromagnetic correlations formed by the spins of the Eu atom, well above the Néel temperature, revealing

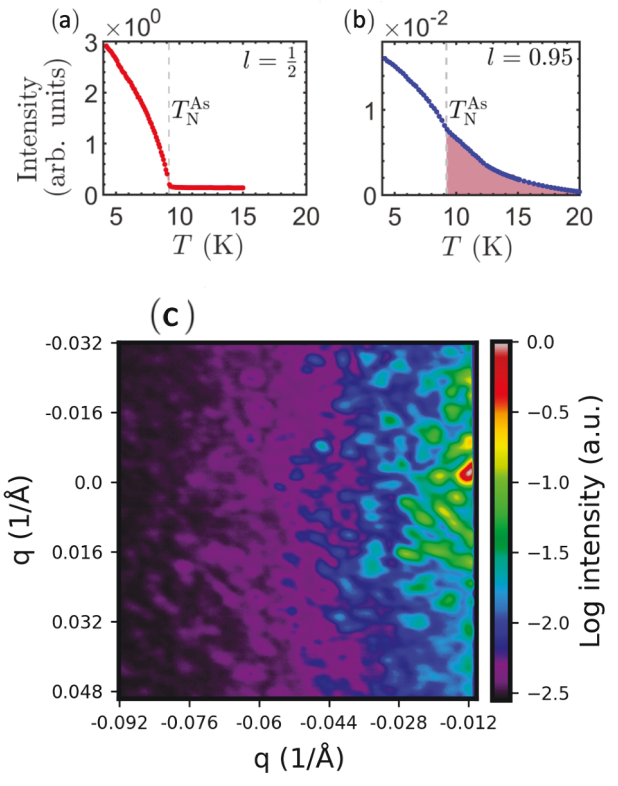

Figure 4. Diffuse magnetic scattering. (a,b) the temperature dependence of the resonant elastic scattering intensity with scattering vector along (0,0,1/2) and (0,0,0.95) in $EuCd_2As_2$, respectively, taken from Soh and co-workers [86]. The increase in diffuse scattering above the Neel temperature T_N coincides with an increase in the in-plane resistivity, suggesting this may be due to charge carrier scattering from ferromagnetic fluctuations of the Eu spins and motivates the investigation of ultrafast spin fluctuations. (c) Diffuse scattering can also be studied in the soft x-ray range such as the resonant speckle pattern shown here, collected at an X-FEL which can be used to study nanosecond spontaneous fluctuations of the prototypical spin-glass system CuMn. The image shows the spin-glass speckle using the XPFS prototype instrument [72]. The image was collected at the *L*–edge resonance for Mn in a forward scattering geometry and demonstrates that magnetism can be extracted on short timescales, even with a large, non-magnetic diffuse scattering background, by the use of resonant scattering.

evidence of short-lived Weyl nodes [86]. The most common method for isolating the magnetic diffuse scattering however has been via polarized neutron scattering [87].

Such methods have also been used in fruitful studies of frustrated magnetism [85]. Just as with polymer glasses, diffuse scattering is vital in studies of spin glasses and quantum spin glasses and liquids, to be able to unravel the nature of the interactions, which are frustrated either geometrically [88] or by introducing site or bond disorder to randomize the exchange interactions [89]. In some cases, variations in the diffuse scattering on very long time scales (10s of minutes) have been observed, with changes failing to stabilize

over several hours in the Ising spin chain $Ca_3Co_2O_6$ [90]. In a similar type of system, γ-CoV_2O_6, similar changes occur but on a much shorter time-scale, with relaxations observed by muon spin rotation decaying over several μs [91]. With neutrons, this time-scale can be pushed shorter using the neutron spin-echo technique to cover ps to 100s of μs. Unfortunately, this method is very flux hungry, with a limited number of instruments around the world possessing these capabilities [32]. These experiments often also indicate that significant dynamical processes exist on sub-picosecond timescales [92].

With x-ray scattering, there are several potential methods to isolate the magnetic diffuse scattering. Polarization can also be used as a tool, but it is more common to exploit resonant elastic x-ray scattering from magnetic ions [86]. Where working at the resonant edge is necessary, to push to the true ultrafast regime requires some of the techniques discussed earlier in this section (see Sec. 2.2 for instance), especially with new electron accelerator technology [93] (see Sec. 5.2.1).

It is also possible to identify positions in reciprocal space where there is no charge scattering. A celebrated example of this in magnetism is the observation of the so-called 'pinch points' that are characteristic of the spin ice state [94]. Here, the spin-$\frac{1}{2}$ neutrons interact directly with the magnetic fields generated by magnetic ions. Such measurements typically take a long time due to the limited neutron flux available, and can usually be considered as long-time averages of the short-range order. As we might expect from the fluctuation-dissipation theorem, this short-range scattering may display dynamics on a range of time scales, depending on the specific origin of the diffuse scattering. This is well studied in soft condensed matter, for example regarding the glass transition in polymers [95], but less so in crystalline materials.

When scattering from different components overlaps in reciprocal space, there is also potential for this to be unraveled by observing different signatures in the time domain [96]. For example, in the spin glass systems, structural or charge scattering can obscure magnetic scattering directly related to the spin structure. In thin films of CuMn, this has been observed by comparing non-resonant to resonant scattering at the Mn-edge as a function of momentum transfer. This was shown to be successful in the measurement of the 4-spin correlation function which displays dynamics on very slow time-scales, at the level of hundreds to thousands of seconds, to determine the Edwards-Anderson order parameter [97]. Diffuse scattering was furthermore measured in a forward scattering geometry at the LCLS, shown in Figure 4b, though this q–range is much less than typical diffuse scattering measurements due to the longer wavelength of soft x-rays. This shows a resonant coherent speckle pattern of the diffuse scattering around $q = 0$ using the XPFS prototype instrument at the LCLS [72]. It was shown that the large amount of diffuse scattering in the spin glass state could be measured out to large q, up to

almost ~ 1 $Å^{-1}$, and could furthermore be captured on the order of one pulse width, about 100 fs. Here, instead of using resonant enhancement to separate the charge and magnetic scattering for extraction of pure spin dynamics, the dynamical signatures of the scattering could be used to measure the dynamic spin component, on top of the static charge contribution. By targeting the many areas which have been addressed above in magnetic neutron diffuse scattering with ultrafast x-rays, a wide ranging and fertile ground is available for exploration.

3 Theory

To take full advantage of the research available with the expanding X-FEL capabilities, certain theoretical tools are vital to tie the methods as outlined above together. Especially due to the notorious scarcity of X-FEL beamtime and experimental complexity of the methods involved. Strong predictive models are needed before and during the experiment to ensure the allocated time is used optimally and efficiently. Furthermore, because of the rich variety of interactions between x-rays and materials, a theoretical perspective is crucial when analyzing data in order to distinguish signal from background. Since the focal point here is on resonant x-ray scattering, we start with an overview of the theoretical background for the magnetic cross-section, with an added discussion of how this relates directly to XPFS, though a full treatment of this will appear elsewhere. This is followed by a discussion of density functional theory (DFT). This acts as the starting point to attain parameters that can be used to build an effective Hamiltonian model, using numerical methods which are outlined in the following section. Numerical methods for simulating strongly correlated spin systems which we focus on here for magnetism, are exact diagnolization (ED) and the density matrix renormalization group (DMRG).

3.1 Magnetic cross-section and resonant XPFS

The main mechanism we will focus on in this article is resonant elastic magnetic scattering. In an experiment this is achieved by tuning the incoming x-ray photon energy to an absorption edge of the metallic ion carrying the magnetic spin-moments originating from unpaired valence electrons. To model this, we typically focus on dipole transitions, though the quadropolar channel can also be studied. The full cross-section for resonant scattering for the electric dipole transitions was first worked out by M. Blume [98] and is given by:

$$f = f_c - if_{m1}(\epsilon_f^* \times \epsilon_i)\cdot\mathbf{s} + f_{m2}(\epsilon_f^* \cdot \mathbf{s})(\epsilon_i \cdot \mathbf{s}) \tag{1}$$

where ϵ represents the incoming and final polarization states, $\mathbf{s}$ is the spin of the atom, and the f_i's are the charge and the first and second order magnetic, frequency-dependent scattering amplitudes.

Typically, in a scattering experiment, we project the cross-section into components that are either in the scattering plane, or orthogonal to the scattering plane. For our purposes here, we tend to focus on the second term, which for small-angle scattering gives only off-diagonal matrix elements for the scattering process [99]:

$$\epsilon_f^* \times \epsilon_i = \begin{pmatrix} \epsilon_\sigma^* \times \epsilon_\sigma & \epsilon_\sigma^* \times \epsilon_\pi \\ \epsilon_\pi^* \times \epsilon_\sigma & \epsilon_\pi^* \times \epsilon_\pi \end{pmatrix} = \begin{pmatrix} 0 & \mathbf{k_i} \\ -\mathbf{k_f} & 0 \end{pmatrix}$$

In this case, the cross-section goes as $\sim \mathbf{k} \cdot \mathbf{s}$ and is optimized for spins pointing out of the sample plane, or parallel to the incoming beam. The resonant intensity enhancement can be several hundredfold that of the non-resonant magnetic contribution, but is still often small compared to the intensity originating from charge-scattering. In practice, it is best to choose Bragg reflections which are forbidden by the space-group of the chemical lattice but allowed by the magnetic sublattice, so that the first term of Equation 1 can be ignored and only the magnetic terms remain.

In order to observe the dynamics associated with the magnetic scatterers as described in Section 2.2 the resultant scattering intensity from Equation 1 is measured as a time-series at a region of interest in reciprocal space q. For a typical XPCS experiment, the intensity-intensity autocorrelation function can be calculated:

$$g_2(q,\tau) = \frac{<I(q,t)I(q,t+\tau)>}{<I(q,t)>^2} \tag{2}$$

where τ is the time difference between intensities at different times, and the brackets designate an average over t. Importantly, this can be cast in terms of the intermediate scattering function by the Siegert relation [100] as:

$$g_2(q,\tau) = 1 + A[S(q,\tau)/S(q)]^2 \tag{3}$$

where the intermediate scattering function is equal to the field-field correlation function, $g_1(q,\tau)$. This holds as long as the scattering being observed is a Gaussian process, with the phase having an equal probability on the range of $\phi \in [0, 2\pi]$ [101]. One note here is that when representing magnetic x-ray scattering, this is not the spin-spin correlation function, which is typically calculated from theory, but the squared amplitude of the spin-spin correlation function, or a 4-spin correlation function. However, one is also able to carry

out so-called 'heterodyne' measurements, and so provide access directly to the spin-spin correlation function [102–104].

For the XPFS measurements mentioned in Sec. 2.2, one additional element is the relationship of the contrast, which can be directly calculated from the summed x-ray pulses, and the correlation function above. An important development in this area was in the demonstration of the equivalence of these two quantities to within a multiplicative factor [71]. This indicates that a contrast measurement is able to retrieve the equivalent information about the intermediate scattering function, as in XPCS.

Lastly, typical experiments rely on both the large pulse energies and the pulse structure of the beam in time, but the scattered photons are usually collected in the sparse limit. In this case, photon counting is necessary to evaluate the contrast. Because the beam is fully coherent, the contrast can be determined by fitting the distribution of photon counts per speckle to the negative binomial distribution, which relates the contrast $C = C(q, \tau)$ to the probability of k–events for a given average intensity, $\overline{k}$:

$$P(k) = A_0(k, M) \left(\frac{\overline{k}}{\overline{k} + M} \right)^k \left(\frac{M}{\overline{k} + M} \right)^M, \tag{4}$$

where $A_0(k, M)$ is a normalization constant which depends on the contrast and the speckle photon density, given by:

$$A_0(k, M) = \frac{\Gamma(k + M)}{\Gamma(M)\Gamma(k + 1)} \tag{5}$$

In Equation 4 and Equation 5, the dependence is expressed as the number of degrees of freedom of the speckle pattern M, or $M = 1/\sqrt{C(q, \tau)}$. Since this equation can not be solved analytically, the parameters of the distribution are usually estimated by invoking estimators that are valid in the low $\overline{k}$ limit [105] or by using maximum likelihood estimation [106]. Under certain conditions, an analytical solution has been shown to exist when multiple k–events are observed [66].

3.2 First-principles approach for modeling quantum magnetism

Next, we outline the theoretical approach to aid these ultrafast experimental methods, which starts with first-principles density functional theory (DFT) based modeling. Beyond phenomenology, ab initio calculations originate from a theoretical perspective which is entirely independent of analysing

experimental data. They offer a logically self-consistent foundation for deducing experimental phenomena, both observed and anticipated. This assists in confirming that the phenomena observed experimentally are indeed physically meaningful. In essence, establishing a road map between theoretical and numerical methods and experimentally observed phenomena enables us to predict new phenomena based on unverified theories or models. This approach fosters the development of valuable experimental conjectures, which can then be taken to the laboratory for verification.

Magnetic properties span a range from fundamental quantum spins to collective, classical spin moments. In the most challenging scenarios, magnetic ordering is deeply linked to spin exchange and/or super-exchange between quantum spins located on various magnetic atoms or orbitals. The dynamics after perturbing these spins reflect the emergent phenomena of strongly correlated systems and can be computed by examining the spin structure factor and spin-spin correlation functions. These observables are not only directly accessible through computation, but are also closely related to measurable properties in the field of ultrafast magnetism.

Simulations of strongly correlated spins often rely on a simple model, described by a Hamiltonian with single-body or many-body interactions, which captures the essence of these correlations. The model parameters for a reliable simulation, such as the short-range or long-range Heisenberg interaction J, are accessible through DFT-based methods. It is worth noting that other analytic methods, such as linear spin wave theory for fitting $S(q,\omega)$ and perturbation theory for deriving exchange coupling strengths, offer multiple approaches that can yield qualitatively similar answers. However, considering the cost of trial and error of doing real experiments an unbiased numerical method like DFT serves as a crucial starting point for providing estimations of a model for further investigations.

The recipe proceeds along the following steps: (1) Advanced density functionals [107,108], such as the recently constructed SCAN functional [109], are used to gain a handle on the ground-state electronic, magnetic, and topological structure. Spin-orbit coupling (SOC) effects can be accounted for in these computations [110]. (2) First-principles spin-resolved band structures and wavefunctions are then used to evaluate magnetic anisotropy energies, magnetic moments, exchange parameters, anisotropic exchange coefficients, and the Dzyaloshinskii-Moriya interaction (DMI) [111–113]. (3) Informed by first-principles results, material-specific, effective tight-binding model Hamiltonians can be constructed for incorporating effects of electron-electron interactions in our modeling. (4) Using atomistic spin dynamics (ASD) simulations with our model Hamiltonians, we can investigate the evolution of skyrmion states in various materials [114,115]. Finally, (5) the

preceding steps can be repeated after revealing effects of strains and magnetic fields on effects such as skyrmion formation.

The modeling of magnetic structures, especially skyrmions, within the DFT framework is quite challenging due to the large size of the magnetic unit cells involved. Therefore a combination of DFT and ASD simulations is needed, for instance, to study DMI-induced skyrmions in the presence of an external magnetic field. This has previously been used in treating CrI_3 [116]. It involves finding the solution to the Landau-Lifshitz-Gilbert (LLG) equation [115]:

$$\frac{dm}{dt} = |\gamma| m \times \nabla \mathcal{H} + \alpha (m \times \frac{dm}{dt}) \tag{6}$$

where γ is the gyromagnetic ratio, m is the total magnetic moment vector for each magnetic atom, α is the Gilbert damping coefficient, and most importantly, $\mathcal{H}$ is the Hamiltonian of the system

$$\mathcal{H} = -\sum_{<ij>} J_{ij} n_i \cdot n_j - \sum_{ij} K_j (\hat{K}_j \cdot n_i)^2 - \sum_i \mu_i B \cdot n_i - \sum_{<ij>} \vec{D}_{ij} \cdot (n_i \times n_j) \tag{7}$$

where J_{ij} is the Heisenberg symmetric exchange, K_j is the single-ion anisotropy, B is the external magnetic field, and D_{ij} is the DMI vector. Note that $\hat{K}_j$ denotes the direction of the anisotropy and $m_i = \mu_i \cdot n_i$ is the magnetic moment.

Once the electronic structure of a given magnetic material within the DFT framework is attained, a highly accurate real-space low-energy model can be constructed using Wannier functions as the basis implemented in the Wannier90 code [117,118]. Green's functions combined with the magnetic force theorem are used to systematically calculate the exchange parameters of the Heisenberg Hamiltonian following the Korotin approach [119]. The isotropic exchange parameters, DMI, and the anisotropic exchange between two sites i and j can be extracted from the following equations.

$$J_{ij} = \mathrm{Im}(A_{ij}^{00} - A_{ij}^{xx} - A_{ij}^{yy} - A_{ij}^{zz}), \tag{8}$$

$$K = Im(A^{uv} + A^{vu}) \tag{9}$$

$$\vec{D}_{ij}^{u} = Re(A_{ij}^{0u} - A_{ij}^{u0}), \tag{10}$$

where $A_{ij}^{uv} = -\frac{1}{\pi}\int_{-\infty}^{E_F} Tr\{\mathbf{p}_i^z \mathbf{G}_{ij}^u \mathbf{p}_j^z \mathbf{G}_{ji}^v\} d\epsilon$, $u, v = \{0, x, y, z\}$, $\mathbf{G}_{ij}$ is the Green's function, and $\mathbf{p}_i = \mathbf{H}_{ii}(R = 0)$ is the intra-atomic part of the Hamiltonian. These magnetic exchange parameters are then used in the ASD simulation to predict the presence of skyrmions. To our satisfaction, this method has been extensively tested for various magnetic materials, such as CrI_3 [116] and $NiPS_3$ [120].

However, since the exchange-correlation energy – which encompasses all spin interactions crucial in magnetism – is treated as a minor modification to the kinetic energy and Coulomb potential, methods based on density functional theory fundamentally underestimate the impact of strongly correlated electron spins. Searching for the global minimum energy that aligns with the precise magnetic structure largely depends on the initial hypothesis of the magnetic structure and the consequential customization of the magnetic unit cell. Prior knowledge, combined with numerous attempts at non-prohibited magnetic structures candidates, will ultimately assist in identifying the most likely correct magnetic structure. Once the magnetic properties are captured, this can inform the subsequent process of applying the Hamiltonian with reasonable model parameters, essential for computing correlation functions and structure factors.

3.3 Numerical methods for strongly correlated systems

The heart of this process, after using first-principles DFT computations as the starting point input, is in using strongly correlated numerical methods. Studying the ground state of an effective model Hamiltonian derived from DFT computations can uncover the low-energy physics in quantum magnetism. The spin interactions in the Hamiltonian are typically strongly correlated, which requires associated methods, such as exact diagonalization (ED) [121], variational Monte Carlo [122–124], and density matrix enormalization group (DMRG) [125], to simulate an accurate ground state of super-exchange electrons.

Since quantum Monte Carlo suffers from the severe 'sign problem' [126,127] at low temperatures and the possible system size can be limited in ED [128], we point out that DMRG can have an impact on the ultrafast study of quantum magnets. DMRG is an unbiased numerical method that is widely used for calculating quantum systems. The second generation DMRG [129–134] is based on the matrix product state (MPS) and matrix product operator (MPO), which for a given Hamiltonian, such as that defined in Equation (7), can precisely encode a MPO. This allows the algorithm to target the true ground state by minimizing the variational ground state energy.

Searching for this ground state of a given Hamiltonian can be costly due to the exponentially increasing Hilbert space with system size. DMRG is a one-dimensional (1D) algorithm, as initially proposed, but has been used to

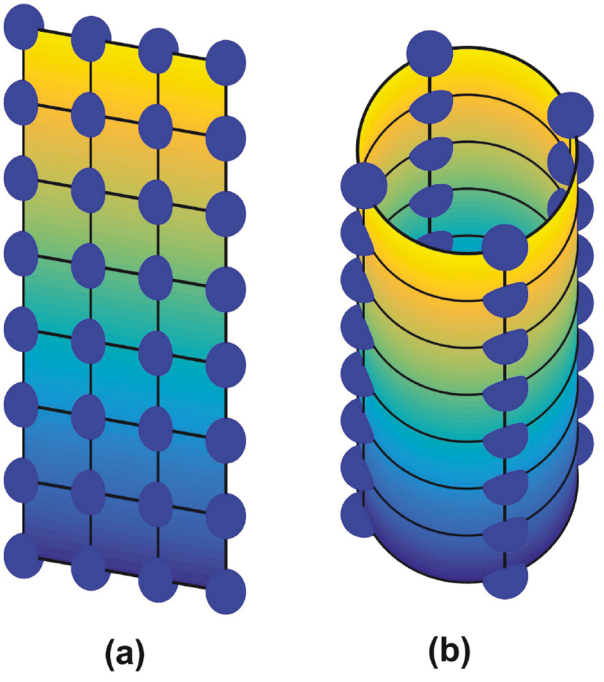

Figure 5. The quasi-one-dimensional system is used for the DMRG calculations. (a) An example of a 4-leg ladder, with extension in the vertical direction. (b) For the computation to mimic the 2D condition, a cylinder geometry allows for a periodic boundary condition in one dimension.

simulate two-dimensional (2D) systems. This is possible by numbering each site of an interacting spin in real space into a sequence so that some of the nearest neighbor spins in real 2D become long-range pairs in the sequence. The approximation is inevitable in DMRG because it prioritizes short-range entanglement. However, the long-range entanglement, if not dominant, can also be truncated to minimize the computational cost. Therefore, DMRG always utilizes a cylinder geometry (as shown in Figure 5) with periodic boundary conditions in one direction to approximate a 2D system so that the nearest neighbor sites will not be separated by a large distance when transforming to the numbered sequence. The realistic 2D system is approached by expanding the cylinder width.

Considering conserved quantum numbers can further reduce the computational cost when approaching larger cylinders with higher accuracy. The constraints rule out unwanted states, such as violation of particle number conservation, so that one can search the variational ground state in a subspace faster. The ground state properties of quantum materials can suffer from finite-size effects, low computational accuracy, or both, so it is highly nontrivial to push the limit of large-scale DMRG calculations to achieve higher accuracy with large system sizes. Further speedup is possible through parallel computing.

Moreover, the dynamical density matrix renormalization group (D-DMRG) [135] is a variational method for calculating the zero-temperature dynamical properties in 1D and quasi-1D quantum many-body systems. Typically, it is given by a dynamical correlation function, defined as

$$G_X(\omega + i\eta) = -\frac{1}{\pi}\langle\psi_0|\hat{X}^\dagger \frac{1}{E_0 + \omega + i\eta - H}\hat{X}|\psi_0\rangle \tag{11}$$

where, $|\psi_0\rangle$ is the ground state and $\hat{X}$ is a quantum operator. However, consider $W_{X,\eta}(\omega, \psi)$ substantively with the formula

$$W_{X,\eta}(\omega, \psi) = \langle\psi|(E_0 + \omega - H)^2 + \eta^2|\psi\rangle + \eta\langle X|\psi\rangle + \eta\langle\psi|X\rangle \tag{12}$$

where $|X\rangle = \hat{X}|\psi_0\rangle$. Then minimizing $W_{X,\eta}(\omega, \psi)$ yields the imaginary part of the dynamical correlation function for $\eta \to 0$, *i.e.*, $I_X(\omega + i\eta) = \text{Im}\, G_X(\omega + i\eta) = -W_{X,\eta}(\omega, \psi_{min})/\pi\eta$. The variational problem for solving $|\psi_{min}\rangle$ is achievable with the standard DMRG.

The zero-temperature time-dependent correlation function, defined as $G_X(t \geq 0) = \langle\psi_0|\hat{X}(t)\hat{X}(0)|\psi_0\rangle$, is solvable through the Laplace transform of a spectral function $G_X(\omega + i\eta)$, or using ED together with time-dependent DMRG [136]. Comparing the calculated results through the numerical techniques discussed here with real experimental data, can help confirm or further modify the microscopic model provided by first-principles DFT calculations, thus cross-validating the reliability of the results from multiple dimensions and improving our comprehension about real physics in the system. Significantly, this type of modeling of magnetic systems has fresh potential for original contributions in further understanding the results using the experimental X-FEL methods described here for the ultrafast regime.

4 Machine learning

In this section, we choose a few instances to review where machine learning (ML) models have been used to aid in the development of the experimental capabilities discussed in this paper. These are in photon detection, learning Hamiltonian parameters, and in experimental steering of advanced experiments, each outlined below.

4.1 Photon detection

One common problem in ultrafast x-ray methods is in single photon detection, where photon detection algorithms can be useful in diffuse scattering for large momenta values (Section 2.3), or in XPFS (Section 2.2). For this, a number of droplet algorithms have been developed which can determine

the photon distribution in the single-photon limit [137–139]. ML algorithms have been designed which have been shown to perform better than any droplet algorithm developed so far. An example is a convolutional neural network (CNN) with an U-Net architecture, which can be trained to photonize raw input speckle patterns for instance, and extract important information under significant levels of electron cloud smearing [106]. For detectors which have small pixels, the smearing can become insurmountable. For instance, not only is the limit of sparse detection possible, in this case down to the level of 1% coverage of photons per pixel, but the CNN is also able to handle bright speckle patterns as well. This is an important example of ML-capabilities which push current limits, as when the electron clouds from the droplets start to coalesce, the traditional droplet algorithm breaks down and is not able to handle the photon density on the detector due to the merging of the electron clouds.

Moreover, it was shown that with this particular algorithm, which uses a regression based ML-approach in which the discrete number of photon counts can be estimated as a continuous value [106], the contrast information could be extracted from regimes which are not possible using direct droplet detection. Another route is to use a CNN to obtain discrete photon maps from our procedure, which is then used to extract the contrast. For this method, the photon assignments are classified into different discrete groups via optimization with the categorical cross-entropy loss function. This predictive classification may provide a better solution to related tasks or functionality with this approach. This topic is beyond the scope of this paper, but is an area of ongoing research.

4.2 Hamiltonian parameter learning and spectra analysis

Another growing area of ML models for scattering experiments and magnetism is in the learning of Hamiltonian parameters from experimental measurements for systems which can be modeled by magnetic spin Hamiltonians. Autoencoder-based machine learning models have been utilized to analyze static structure factors $S(\mathbf{q})$ measured with neutron scattering on the spin ice system $Dy_2Ti_2O_7$ for instance, to extract their model parameters [140–142]. The autoencoder-based method was later extended to extract the dynamical structure factor $S(\mathbf{q}, \omega)$ for α-$RuCl_3$ [143].

However, a prime example of combining ML with theory and experiment is the following. Mainly used in computational photography, neural implicit representations have been applied to spectroscopy experiments and were used to interpret the dynamical structure factor $S(\mathbf{q}, \omega)$ of a square-lattice spin-1 antiferromagnet La_2NiO_4 [144]. A ML-model has been constructed to train on many spin-wave spectra to learn how to predict spectra for a given Hamiltonian model based on input energy-momentum coordinates $(\mathbf{q}, \omega)$

and Hamiltonian parameters (J, J_p). The trained ML-model was then utilized to extract Hamiltonian parameters from measured spectra. This was validated by comparing to inelastic neutron scattering data [145] and confirming this ML approach experimentally in the presence of background and noise. This is an example of how all three compoments, theory, ML, and experiments can be combineed to make progress in this area. We note that ultrafast does not have meaning in neutron scattering at present, but methods such as XPFS are closely related and can be thought of as an x-ray version of high resolution spectroscopy by studying ultrafast fluctuations. This ML approach can impact this, as well as the other ultrafast methods, outlined here.

Apart from parameter learning, ML models have further been useful in other spectra analysis tasks. For example, convolutional neural networks (CNN) have been applied to identify what spin model type yields a given spectra, where a variational autoencoder (VAE) can be applied to remove noise or enhance physical signals [146]. This ML-assisted denoising idea is further developed with a more advanced ML model originally invented for image-to-image translation, dual contrastive learning GAN (DCLGAN) [147], to bridge noisy experimental images and clean simulated images [148].

4.3 Experimental steering

The last area we want to introduce here, which can be bolstered in ultrafast X-ray magnetism, is in the use of ML-augmented experimental steering. The sequential Bayesian experimental design for instance makes use of previously measured information to guide subsequent measurements [149–151], which has achieved success in various types of experiments [152–154]. In particular, this method is important for large-scale X-FEL facilities, where data can be collected and fed into the model to make the best guess for deciding which measurements to make for an experiment. At the least, this will allow one to measure the most important data points in a large space of experimental settings, which can be used to choose the next data collection point that provides maximized information gain, effectively steering the data collection process. The applications of Bayesian design methods to complex spin systems are still limited given expensive forward calculations for spin model Hamiltonians. ML methods such as neural networks can be trained to serve as a surrogate model of the original model prior to experiments, allowing for rapid and scalable forward model computations required in such Bayesian design methods during collecting experimental data. This has been shown to work in steering simulated XPFS measurements for spin excitations in 2D van der Waals magnets [155], which enables real-time model parameter estimations and physics model-informed experimental planning for maximized beam time efficiency.

5 Outlook

5.1 Scientific prospects

With the ultrafast experimental methods outlined here, the prospects for new routes towards understanding magnetism are numerous. The energy probed with THz excitation enables a variety of low-energy states to be excited and probed directly, especially with resonant x-ray scattering. This precision for capturing emergence and collective excitations will be particular useful for systems that exhibit strong correlation, such as in Mott-physics, unconventional or topological superconductivity, or complex magnetic textures, such as chiral phases, magnetic nematics, or skyrmions phases. By new developments with the pulse structure used at X-FELs, x-ray scattering can be used to study spontaneous fluctuations in the natural ground state of magnetic and 'magnetic-like' systems. This opens wide a new era of ground state fluctuations and offers the ability to directly compare to theoretical modeling of exchange parameters for instance. Finally, diffuse scattering on ultrafast timescales can also offer new features for the field of magnetism by extending the studies to short range ordered structures, especially in systems that host a large degree of magnetic frustration, or those with short correlation lengths, such as in low-dimensional spin chains, spin-glasses, or quantum spin liquids. To maximize the potential of these techniques for the future, we discuss in the following special modes of ultrafast x-ray experiments. We conclude this future outlook with a description about novel instrumentation, and current instruments presently being constructed at the LCLS-II.

5.2 Special accelerator modes

Generating different x-ray pulse separation times for performing probe-probe such as XPFS, or x-ray pump / x-ray probe studies as mentioned earlier, is important for executing the ultrafast methods outlined in this paper. This can be accomplished by either optics or special pulse modes developed at the accelerator. Though a large effort has been put into the use of x-ray optics for this task and research progress is tremendous [74], here we outline the two most valuable modes in the soft x-ray regime which will be important for the scientific outlook in ultrafast magnetism.

5.2.1 Fresh-slice x-ray pairs

The fresh-slice scheme [156] can produce pairs of high-power femtosecond x-ray pulses, with simple control of their wavelength and delay. The scheme is based on controlling which temporal slice of an electron bunch lases in a section of the undulator line. This is typically achieved by tilting the electron bunch and subsequently controlling the bunch trajectory. Lasing slices can be

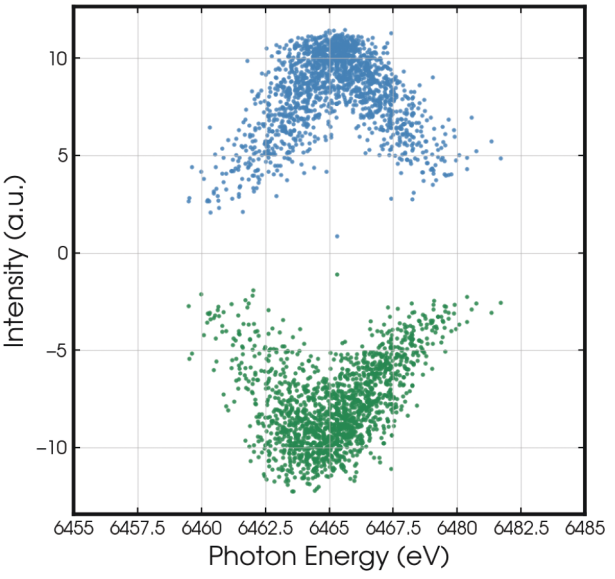

Figure 6. Two-pulse correlation using the 'two-bucket' X-FEL mode. The pulse energy of each pulse is shown, one pulse for each radio frequency bucket of the accelerator. The first pulse, colored in green, is plotted negative for added clarity. The two peaks are aligned at the same energy, showing they have the same color wavelength and can arbitrarily be delayed by integer radio frequency bucket values of 350 ps each.

a couple of femtosecond short, and wavelengths are controlled by the undulator strength in each section, enabling color separation ranging from being at the same wavelength to larger than a factor 2. The maximum delay depends on the strength of an intra-undulator line magnetic chicane. Practically, the scheme has been demonstrated for delays up to 1 picosecond. Temporal coincidence, or exchanging the arrival time of the two pulses, is possible if the slice on the tail is set to lase in the upstream undulator section.

5.2.2 Two-bunch x-ray pairs

For longer delays, ranging from hundreds of picoseconds to hundreds of nanoseconds, two separate electron bunches are extracted at the cathode, accelerated and compressed in the linear accelerator and lase in the undulator line [93]. The unitary time separation depends on the accelerator RF frequency; for the LCLS S-Band linac, it is close to 350 picoseconds. Performance for each bunch can be similar to that of a regular, single bunch SASE pulse. Typically, the two-bucket scheme is set up to have both pulses lasing at the same wavelength, but a small color separation is achievable by having the two electron bunches at slightly different energies. For instance, Figure 6 shows the pulse energy of each pulse in a dispersive location of the accelerator, with a positive correlation. This can be used to adjust the color of each pulse to have the same wavelength as well as equal pulse energies.

5.3 State-of-the-art instrumentation

Currently, new instruments around the world are being developed to take full advantage of these ultrafast X-ray scattering techniques in the area of magnetism. For instance, at the SwissFEL, the XFEL facility of the Paul Scherrer Institute in Switzerland, the newly commissioned soft X-ray Furka endstation is capable of resonant elastic and inelastic X-ray scattering experiments with the inclusion of THz-pump for time-resolved studies from 400–1900 eV [157]. It is complemented by the Bernina endstation, which possesses similar experimental capabilities at hard X-ray energies (2,000-13,000 eV) [158]. For example, these instruments have been applied to study spin-lattice interactions of electromagnons [159] and quenched lattice fluctuations in optically-driven $SrTiO_3$ [160]. At the Bernina instrument, the high-field THz and resonant diffraction cryo-chamber is capable of cooling the sample environment down to 5 K. The availability of *in-situ* liquid He cryo-coolers in the latest generation of X-FEL endstations is crucial for studying magnetic phases in their ground states without the disturbance of thermal excitations.

In addition, high-repetition rate machines such as the European X-FEL [161] are already taking full advantage of the latest generation of instruments which can host the necessary infrastructure and technology for using these types of methods. For instance, at the SLAC National Accelerator Laboratory, the new accelerator for the LCLS-II will soon provide up to nearly ~1 MHz repetition rate with an array of possible pumping schemes, including THz, with new instruments currently being designed, constructed, and commissioned. Some efforts have been made to retrofit current x-ray instruments, as well as the development of full-scale instruments designed for the purpose of carrying out XPFS measurements in the soft x-ray regime for a variety of different geometries. We outline two such cases here. The first is the modification of the so-called chemRIXS instrument, recently modified to carry out XPFS studies on materials, while the second is a future instrument currently under construction.

5.3.1 The chemRIXS instrument for materials

As a first test case, we have developed a capability to take advantage of the recent endstation developed as part of the LCLS-II suite of instruments focused on ultrafast chemical science, specifically in x-ray absorption spectroscopy and resonant inelastic x-ray scattering, the so-called 'chemRIXS' instrument. This is specifically focused on using liquid jet or liquid sheet jet systems for the study of ultrafast physics and chemistry experiments [162]. The spectrum of the molecules illuminated in the solvent can be optically excited and

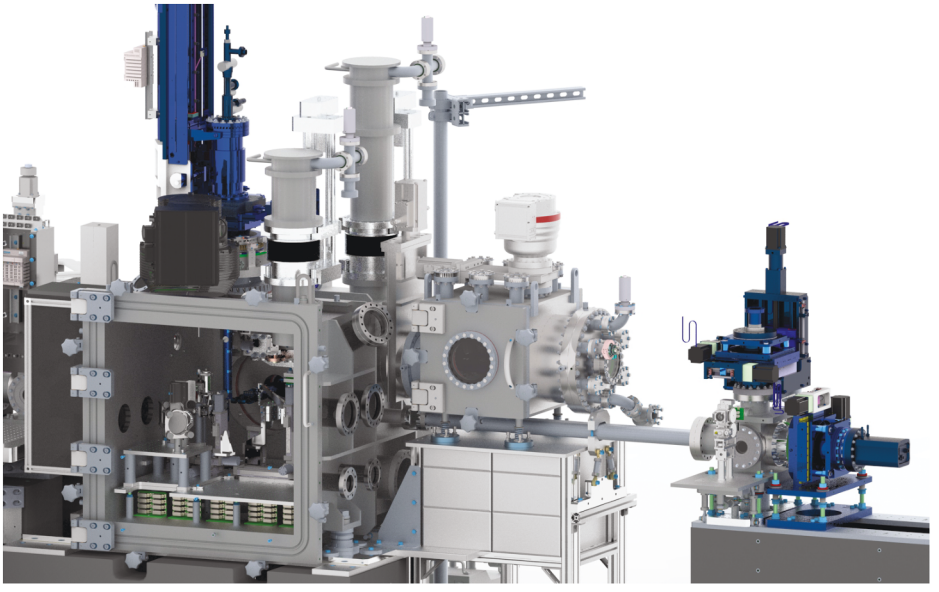

Figure 7. The chemRIXS endstation with the enhancements designed for XPFS measurements on solids. The main sample chamber (left) houses the liquid jet system or solid material sample. The electromagnet is inserted perpendicular to the beam horizontally, while the detector and mask assembly (right) are placed in the forward scattering direction for transmission geometry measurements. All dark blue color-coding designate components that were designed for the thin film, ultrafast magnetism experiments.

the chemical structure evolution can be followed on the time-scale of these chemical changes [163].

While not designed for solid material samples, some instrumentation enhancements were made such that first XPFS experiments could be performed on the newly designed beamline. This was carried out on thin film magnets by designing and fabricating a solid sample holder to replace the liquid jet, a mounted CCD detector, together with a detector mask, and a manipulator to control the placement of an electromagnet. The mask was used to limit the area of illumination on the detector chip to enable higher speed readout [79]. This feature can be adjusted, i.e. to collect a larger fraction of the speckle pattern and a slower rate, depending on the experimental system. The detector was placed in a forward scattering geometry, compatible with the chemRIXS set-up. This detector scheme implemented for this set of experiments has been described in detail elsewhere as a prototype XPFS instrument [72], but was here used in conjunction with the liquid jet endstation. An overview of this set-up in this configuration is shown in Figure 7. For a close-up view inside the system, a rendition of the chemRIXS setup from inside the chamber, emphasizing the cryostat and the electromagnetic for magnetic field dependent studies, is shown in Figure 8.

Figure 8. The chemRIXS instrument close-up view inside the sample chamber. This chamber was modified to house an electromagnet and cryostat sample holder to perform XPFS studies on solids.

5.3.2 Future capabilities

Looking forward to future capabilities, LCLS-II beamlines are already in use with new instruments on the horizon. For THz pump/ magnetic scattering probe studies or ultrafast magnetic diffuse x-ray scattering for instance, the latest capability will occur with the commissioning of the qRIXS instrument.

The qRIXS instrument hosts a sample chamber and a rotatable spectrometer consisting of grating and high-speed 2D detector covering the range of scattering angles from 40–150 degrees in the horizontal scattering geometry. The spectrometer is designed to achieve an energy resolution of ~35 meV at 1 keV. The sample chamber is designed to support elastic soft x-ray diffraction. The chamber is equipped with an in-vacuum diffractometer with a 6-axis degree of freedom of motion. Sample cooling down to about 25 K will be possible with the cryogenic sample installation. The ability to introduce oversized optics for long-wavelength THz beams, will be accommodated in the near future [46,61,64].

In addition, we are developing another capability to be able to carry out XPFS measurements in the soft x-ray regime as well (see Figure 9). The focal point of this instrument will be the in-vacuum, long distance, and movable detector motion. This will incorporate the 'ePixM' series designed at Stanford University and SLAC National Laboratory. This will be a large, pixelated detector that can count single photons down to the carbon edge (~285 eV) and will operate at the full repetition rate of the new, superconducting accelerator, at 929 kHz. The instrument, which is still under construction currently, will be capable of moving the detector about a limited scattering angle range while in UHV conditions, with the use of precision laser trackers. It will be housed in a small vacuum chamber and stand with air bearings for chamber motion. An advanced laser tracker system will place the detector coordinates

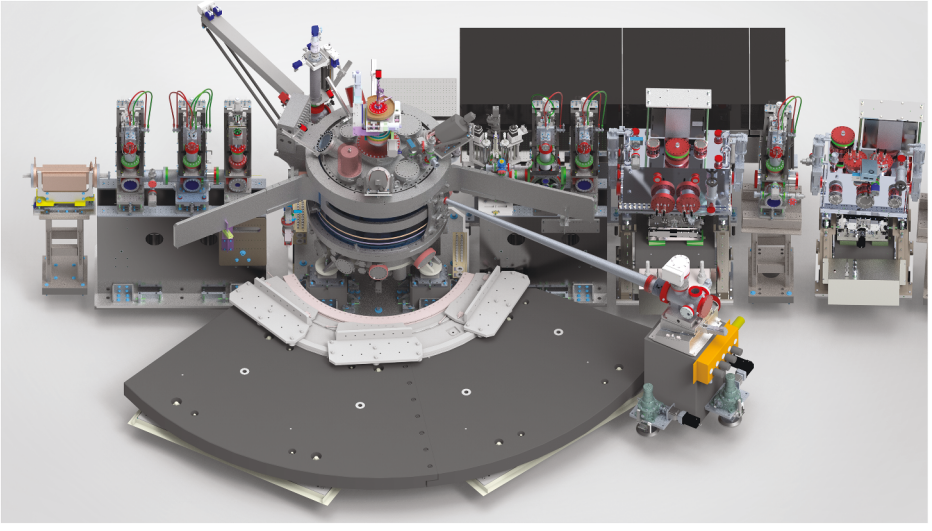

Figure 9. XPFS instrument. The image shows a rendition of the XPFS chamber housing the fast, pixelated detector, on its own movable stand. The scattering path is evacuated at UHV conditions after precision alignment. The whole apparatus mounts to the qRIXS sample chamber, and is part of the NEH 2.2 instrument at the LCLS-II, shown here installed on the beamline. The instrument is still currently under construction.

in the correct geometry at a sample-to-detector distance of about 3 m. Once aligned, a scattering path length drift tube will be attached from the sample chamber, using a rotary seal, to the detector chamber. It will be evacuated to UHV conditions to accommodate soft x-ray scattering in the area of quantum materials. Once complete, this will offer the potential for first XPFS measurements with soft x-rays at an arbitrary scattering angle, important for a myriad of quantum materials and other types of studies on solids.

6 Conclusion

In conclusion, with the latest developments at XFEL sources, studies in ultrafast magnetism are ripe for a renewed focus across many areas of research. We have targeted three new areas that are continued to be developed and will help to capitalize on fresh capabilities to spur magnetic studies in both equilibrium and non-equilibrium investigations. Combining these advanced methods with the latest progress in condensed matter theory and machine learning, the synergy and progress capable in the future for ultrafast magnetism is bright.

Acknowledgments

A special thank you to Prof. Francesc Roig for his invaluable help and guidance. This work was primarily supported by the U.S. Department of Energy, Office of Science, Basic Energy Sciences under Award No. DE-SC0022216. Portions of this work were also supported by the U. S. Department of Energy, Office of Science, Basic Energy Sciences, Materials Sciences and

Engineering Division, under Contract DE-AC02-76SF00515. The use of the Linac Coherent Light Source (LCLS), SLAC National Accelerator Laboratory, is also supported by the DOE, Office of Science under the same contract. S. A. M. acknowledges support by the U. S. Office of Naval Research, In-House Lab Independent Research program. S.K., P.F., and S.R. acknowledge support by the U.S. Department of Energy, Office of Science, Office of Basic Energy Sciences, Materials Sciences and Engineering Division under Contract No. DE-AC02-05-CH11231 (NEMM program MSMAG). The research at Lund University was supported in part by the Swedish Research Council (Award No. 2018-04704). The research at UCSD was supported by the National Science Foundation under Grant No. 2105401. J. J. Turner acknowledges support from the U.S. DOE, Office of Science, Basic Energy Sciences through the Early Career Research Program.

Disclosure statement

No potential conflict of interest was reported by the author(s).

References

[1] Tokura Y, Kawasaki M, Nagaosa N. Emergent functions of quantum materials. Nat Phys. 2017;13:1056–1068. doi: 10.1038/nphys4274
[2] Keimer B, Moore J. The physics of quantum materials. Nat Phys. 2017;13:1045–1055. doi: 10.1038/nphys4302
[3] Giustino F, Lee JH, Trier F, et al. The 2021 quantum materials roadmap. J Phys Mater. 2021;3:042006. doi: 10.1088/2515-7639/abb74e
[4] Cao Y, Fatemi V, Fang S, et al. Unconventional superconductivity in magic-angle graphene superlattices. Nature. 2018;556:43–50. doi: 10.1038/nature26160
[5] Žutić I, Fabian J, Sarma SD. Spintronics: fundamentals and applications. Rev Mod Phys. 2004;76:323. doi: 10.1103/RevModPhys.76.323
[6] Hirohata A, Yamada K, Nakatani Y, et al. Review on spintronics: principles and device applications. J Magnet Magnetic Mater. 2020;509:166711. doi:10.1016/j.jmmm.2020.166711
[7] Opherden D, Tepaske MSJ, Bärtl F, et al. Field-tunable berezinskii-kosterlitz-thouless correlations in a heisenberg magnet. Phys Rev Lett. 2023;130:086704. doi: 10.1103/PhysRevLett.130.086704
[8] Du L, Hasan T, Castellanos-Gomez A, et al. Engineering symmetry breaking in 2d layered materials. Nat Rev Phys. 2021;3:193–206. doi: 10.1038/s42254-020-00276-0
[9] Gong C, Zhang X. Two-dimensional magnetic crystals and emergent heterostructure devices. Science. 2019;363:eaav4450. doi: 10.1126/science.aav4450
[10] Bogdanov AN, Rößler UK. Chiral symmetry breaking in magnetic thin films and multilayers. Phys Rev Lett. 2001;87:037203. doi: 10.1103/PhysRevLett.87.037203
[11] Sie EJ, Nyby CM, Pemmaraju C, et al. An ultrafast symmetry switch in a weyl semimetal. Nature. 2019;565:61–66. doi: 10.1038/s41586-018-0809-4
[12] Qian X, Liu J, Fu L, et al. Quantum spin hall effect in two-dimensional transition metal dichalcogenides. Science. 2014;346:1344–1347. doi: 10.1126/science.1256815
[13] Liu Y, Li Y, Rajput S, et al. Tuning dirac states by strain in the topological insulator bi2se3. Nat Phys. 2014;10:294–299. doi: 10.1038/nphys2898
[14] Oka T, Aoki H. Photovoltaic hall effect in graphene. Phys Rev B. 2009;79:081406. doi: 10.1103/PhysRevB.79.081406

[15] Wandel S, Boschini F, da Silva Neto EH, et al. Enhanced charge density wave coherence in a light-quenched, high-temperature superconductor. Science. 2022;376:860–864. doi: 10.1126/science.abd7213
[16] Tengdin P, You W, Chen C, et al. Critical behavior within 20 fs drives the out-of-equilibrium laser-induced magnetic phase transition in nickel. Sci Adv. 2018;4:eaap9744. doi: 10.1126/sciadv.aap9744
[17] Shan J-Y, Ye M, Chu H, et al. Giant modulation of optical nonlinearity by floquet engineering. Nature. 2021;600:235–239. doi: 10.1038/s41586-021-04051-8
[18] Joy P, Vasudevan S. Magnetism in the layered transition-metal thiophosphates m ps 3 (m= mn, fe, and ni). Phys Rev B. 1992;46:5425. doi: 10.1103/PhysRevB.46.5425
[19] Wildes AR, Simonet V, Ressouche E, et al. Magnetic structure of the quasi-two-dimensional antiferromagnet nips 3. Phys Rev B. 2015;92:224408. doi: 10.1103/PhysRevB.92.224408
[20] Burch KS, Mandrus D, Park J-G. Magnetism in two-dimensional van der waals materials. Nature. 2018;563:47–52. doi: 10.1038/s41586-018-0631-z
[21] Finocchio G, Büttner F, Tomasello R, et al. Magnetic skyrmions: from fundamental to applications. J Phys D Appl Phys. 2016;49:423001. doi: 10.1088/0022-3727/49/42/423001
[22] Mühlbauer S, Binz B, Jonietz F, et al. Skyrmion lattice in a chiral magnet. Science. 2009;323:915–919. doi: 10.1126/science.1166767
[23] Bogdanov A, Hubert A. Thermodynamically stable magnetic vortex states in magnetic crystals. J Magnet Magnetic Mater. 1994;138:255–269. doi: 10.1016/0304-8853(94)90046-9
[24] Li Q, Stoica VA, Paściak M, et al. Subterahertz collective dynamics of polar vortices. Nature. 2021;592:376–380. doi: 10.1038/s41586-021-03342-4
[25] Ament LJ, Van Veenendaal M, Devereaux TP, et al. Resonant inelastic x-ray scattering studies of elementary excitations. Rev Mod Phys. 2011;83:705. doi: 10.1103/RevModPhys.83.705
[26] Paris E, Nicholson CW, Johnston S, et al. Probing the interplay between lattice dynamics and short-range magnetic correlations in $cugeo_3$ with femtosecond rixs. Npj Quantum Mater. 2021;6:51. doi: 10.1038/s41535-021-00350-5
[27] Mazzone DG, Meyers D, Cao Y, et al. Laser-induced transient magnons in $sr_3ir_2o_7$ throughout the brillouin zone. Proc Natl Acad Sci USA. 2021;118:e2103696118. doi: 10.1073/pnas.2103696118
[28] Parchenko S, Paris E, McNally D, et al. Orbital dynamics during an ultrafast insulator to metal transition. Phys Rev Res. 2020;2:023110. doi: 10.1103/PhysRevResearch.2.023110
[29] Dean M, Cao Y, Liu X, et al. Ultrafast energy- and momentum-resolved dynamics of magnetic correlations in the photo-doped mott insulator sr_2iro_4. Nat Mater. 2016;15:601. doi: 10.1038/nmat4641
[30] Mühlbauer S, Honecker D, Périgo EA, et al. Magnetic small-angle neutron scattering. Rev Mod Phys. 2019;91:015004. doi: 10.1103/RevModPhys.91.015004
[31] Hauser W, Feshbach H. The inelastic scattering of neutrons. Phys Rev. 1952;87:366–373. doi: 10.1103/PhysRev.87.366
[32] Gardner J, Ehlers G, Faraone A, et al. High-resolution neutron spectroscopy using backscattering and neutron spin-echo spectrometers in soft and hard condensed matter. Nat Rev Phys. 2020;2:103–116. doi: 10.1038/s42254-019-0128-1
[33] Soda M, Forgan E, Blackburn E, et al. Asymmetric slow dynamics of the skyrmion lattice in mnsi. Nat Phys. 2023;19:1476–1481. doi: 10.1038/s41567-023-02120-5

[34] Kirilyuk A, Kimel AV, Rasing T. Ultrafast optical manipulation of magnetic order. Rev Mod Phys. 2010;82:2731. doi: 10.1103/RevModPhys.82.2731
[35] Beaurepaire E, Merle J-C, Daunois A, et al. Ultrafast spin dynamics in ferromagnetic nickel. Phys Rev Lett. 1996;76:4250. doi: 10.1103/PhysRevLett.76.4250
[36] Siegmann H, Garwin E, Prescott C, et al. Magnetism with picosecond field pulses. J Magnet Magnetic Mater. 1995;151:L8–L12. doi: 10.1016/0304-8853(95)00602-8
[37] Malvestuto M, Ciprian R, Caretta A, et al. Ultrafast magnetodynamics with free-electron lasers. J Phys Condens Matter. 2018;30:053002. doi: 10.1088/1361-648X/aaa211
[38] Jeppson S, Kukreja R. Capturing ultrafast magnetization phenomenon using femtosecond x rays. APL Mater. 2021;9:100702. doi: 10.1063/5.0054006
[39] Dürr H. The x-ray view of ultrafast magnetism. In: Jaeschke EJ, Khan S, Schneider JRHastings JB, editors. Synchrotron light sources and Free-Electron Lasers: accelerator physics, instrumentation and science applications. Cham: Springer International Publishing; 2020. p. 2115–2130. doi: 10.1007/978-3-030-23201-6_50
[40] Bostedt C, Boutet S, Fritz DM, et al. Linac coherent light source: the first five years. Rev Mod Phys. 2016;88:015007. doi: 10.1103/RevModPhys.88.015007
[41] March A, Pratt S, Southworth S, et al. Femtosecond electronic response of atoms to ultra-intense x-rays. Nature. 2010;466:56–61. doi: 10.1038/nature09177
[42] Gomez LF, Ferguson KR, Cryan JP, et al. Shapes and vorticities of superfluid helium nanodroplets. Science. 2014;345:906–909. doi: 10.1126/science.1252395
[43] Glownia JM, Cryan J, Andreasson J, et al. Time-resolved pump-probe experiments at the lcls. Opt Express. 2010;18:17620–17630. doi: 10.1364/OE.18.017620
[44] Bernitt S, Brown GV, Rudolph JK, et al. An unexpectedly low oscillator strength as the origin of the fe xvii emission problem. Nature. 2012;492:225–228. doi: 10.1038/nature11627
[45] Vinko SM, Ciricosta O, Cho BI, et al. Creation and diagnosis of a solid-density plasma with an x-ray free-electron laser. Nature. 2012;482:59–62. doi: 10.1038/nature10746
[46] Kubacka T, Johnson JA, Hoffmann MC, et al. Large-amplitude spin dynamics driven by a thz pulse in resonance with an electromagnon. Science. 2014;343:1333–1336. doi: 10.1126/science.1242862
[47] Beaud P, Caviezel A, Mariager SO, et al. A time-dependent order parameter for ultrafast photoinduced phase transitions. Nat Mater. 2014;13:923–927. doi: 10.1038/nmat4046
[48] Mankowsky R, Subedi A, Först M, et al. Nonlinear lattice dynamics as a basis for enhanced superconductivity in YBa2Cu3O6.5. Nature. 2014;516:71–73. doi: 10.1038/nature13875
[49] Boutet S, Lomb L, Williams GJ, et al. High-resolution protein structure determination by serial femtosecond crystallography. Science. 2012;337:362–364. doi: 10.1126/science.1217737
[50] Chapman HN, Fromme P, Barty A, et al. Femtosecond x-ray protein nanocrystallography. Nature. 2011;470:73–77. doi: 10.1038/nature09750
[51] White WE, Robert A, Dunne M. The linac coherent light source. J Synchrotron Radiat. 2015;22:472–476. doi: 10.1107/S1600577515005196
[52] Altarelli M. The european x-ray free-electron laser facility in hamburg. Nucl Instruments Methods Phys Res Sect Beam Interact Mater Atoms. 2011;269:2845–2849. doi: 10.1016/j.nimb.2011.04.034
[53] Schoenlein R, Boutet S, Minitti M, et al. The linac coherent light source: recent developments and future plans. Appl Sci. 2017;7:850. doi: 10.3390/app7080850

[54] Caviglia A, Först M, Scherwitzl R, et al. Photoinduced melting of magnetic order in the correlated electron insulator ndnio 3. Phys Rev B. 2013;88:220401. doi: 10.1103/PhysRevB.88.220401
[55] Lee WS, Chuang YD, Moore RG, et al. Phase fluctuations and the absence of topological defects in a photo-excited charge-ordered nickelate. Nat Commun. 2012;3:838. doi: 10.1038/ncomms1837
[56] Chuang YD, Lee WS, Kung YF, et al. Real-time manifestation of strongly coupled spin and charge order parameters in stripe-ordered la1.75sr0.25nio4 nickelate crystals using time-resolved resonant x-ray diffraction. Phys Rev Lett. 2013;110:127404. doi: 10.1103/PhysRevLett.110.127404
[57] Först M, Frano A, Kaiser S, et al. Femtosecond x rays link melting of charge-density wave correlations and light-enhanced coherent transport in $YBa_2Cu_3o_{6.6}$. Phys Rev B. 2014;90:184514. doi: 10.1103/PhysRevB.90.184514
[58] Först M, Tobey RI, Wall S, et al. Driving magnetic order in a manganite by ultrafast lattice excitation. Phys Rev B. 2011;84:241104. doi: 10.1103/PhysRevB.84.241104
[59] Forst M, Caviglia AD, Scherwitzl R, et al. Spatially resolved ultrafast magnetic dynamics initiated at a complex oxide heterointerface. Nat Mater. 2015;14:883–888. doi: 10.1038/nmat4341
[60] Shen L, Mack SA, Dakovski G, et al. Decoupling spin-orbital correlations in a layered manganite amidst ultrafast hybridized charge-transfer band excitation. Phys Rev B. 2020;101:201103. doi: 10.1103/PhysRevB.101.201103
[61] Hoffmann MC, Turner JJ. Ultrafast x-ray experiments using terahertz excitation. Synchrotron Radiat News. 2012;25:17–24. doi: 10.1080/08940886.2012.663318
[62] Dakovski GL, Lee W-S, Hawthorn DG, et al. Enhanced coherent oscillations in the superconducting state of underdoped $YBa_2Cu_3o_{6+x}$ induced via ultrafast terahertz excitation. Phys Rev B. 2015;91:220506. doi: 10.1103/PhysRevB.91.220506
[63] Dakovski GL, Heimann P, Holmes M, et al. The soft x-ray research instrument at the linac coherent light source. J Synchrotron RAD. 2015;22:498–502. doi: 10.1107/S160057751500301X
[64] Turner JJ, Dakovski GL, Hoffmann M, et al. Combining thz laser excitation with resonant soft x-ray scattering at the linac coherent light source. J Synchrotron RAD. 2015;22:621–625. doi: 10.1107/S1600577515005998
[65] Schlotter WF, Turner JJ, Rowen M, et al. The soft x-ray instrument for materials studies at the linac coherent light source x-ray free-electron laser. Rev Sci Instrum. 2012;83:043107–043107–10. doi: 10.1063/1.3698294
[66] Shen L, Seaberg M, Blackburn E, et al. A snapshot review—fluctuations in quantum materials: from skyrmions to superconductivity. MRS Adv. 2021;6:221–233. doi: 10.1557/s43580-021-00051-y
[67] Sutton M. A review of x-ray intensity fluctuation spectroscopy. C R Physique. 2008;9:657. doi: 10.1016/j.crhy.2007.04.008
[68] Sinha SK, Jiang Z, Lurio LB. X-ray photon correlation spectroscopy studies of surfaces and thin films. Adv Mater. 2014;26:7764–7785. doi: 10.1002/adma.201401094
[69] Bandyopadhyay R, Gittings AS, Suh SS, et al. Speckle-visibility spectroscopy: a tool to study time-varying dynamics. Rev Sci Instrument. 2005;76:093110. doi: 10.1063/1.2037987
[70] Decaro C, Karunaratne V, Bera S, et al. X-ray speckle visibility spectroscopy in the single-photon limit. J Synchrotron RAD. 2014;20:332. doi: 10.1107/S0909049512051825
[71] Gutt C, Stadler L-M, Duri A, et al. Measuring temporal speckle correlations at ultrafast x-ray sources. Opt Express. 2009;17:55–61. doi: 10.1364/OE.17.000055

[72] Assefa TA, Seaberg MH, Reid AH, et al. The fluctuation–dissipation measurement instrument at the linac coherent light source. Rev Sci Instrument. 2022;93:083902. doi: 10.1063/5.0091297
[73] Esposito V, Zheng XY, Seaberg MH, et al. Skyrmion fluctuations at a first-order phase transition boundary. Appl Phys Lett. 2020;116:181901. doi: 10.1063/5.0004879
[74] Sun Y, Wang N, Song S, et al. Compact hard x-ray split-delay system based on variable-gap channel-cut crystals. Opt Lett. 2019;44:2582–2585. doi: 10.1364/OL.44.002582
[75] Seaberg MH, Holladay B, Montoya SA, et al. Spontaneous fluctuations in a magnetic fe/gd skyrmion lattice. Phys Rev Res. 2021;3:033249. doi: 10.1103/PhysRevResearch.3.033249
[76] Lee JCT, Chess JJ, Montoya SA, et al. Synthesizing skyrmion bound pairs in fe-gd thin films. Appl Phys Lett. 2016;109:022402. doi: 10.1063/1.4955462
[77] Montoya SA, Couture S, Chess JJ, et al. Tailoring magnetic energies to form dipole skyrmions and skyrmion lattices. Phys Rev B. 2017;95:024415. doi: 10.1103/PhysRevB.95.024415
[78] Montoya SA, Couture S, Chess JJ, et al. Resonant properties of dipole skyrmions in amorphous fe/gd multilayers. Phys Rev B. 2017;95:224405. doi: 10.1103/PhysRevB.95.224405
[79] Seaberg MH, Holladay B, Lee JCT, et al. Nanosecond x-ray photon correlation spectroscopy on magnetic skyrmions. Phys Rev Lett. 2017;119:067403. doi: 10.1103/PhysRevLett.119.067403
[80] Weber T, Fobes DM, Waizner J, et al. Topological magnon band structure of emergent landau levels in a skyrmion lattice. Science. 2022;375:1025–1030. doi: 10.1126/science.abe4441
[81] Mangu A, Stoica VA, Zheng H, et al. Hidden non-equilibrium pathways towards crystalline perfection. 2024. Available from: arXiv:2402.04962[cond-mat.mtrl-sci]
[82] Trigo M, Fuchs M, Chen J, et al. Fourier-transform inelastic X-ray scattering from time- and momentum-dependent phonon–phonon correlations. Nat Phys. 2013;9:790–794. doi: 10.1038/nphys2788
[83] Blackburn E, Goodkind JM, Sinha SK, et al. Absence of a low-temperature anomaly in the Debye-Waller factor of solid He^4 down to 140 mK. Phys Rev B. 2007;76:024523. doi: 10.1103/PhysRevB.76.024523
[84] Long MW, Moze O. Magnetic diffuse scattering and the triple-q structure in fcc γ-mnni. J Phys Condens Matter. 1990;2:6013. doi: 10.1088/0953-8984/2/27/008
[85] Long MW. Magnetic diffuse scattering: a theorist's perspective. 1996. Available from: https://inis.iaea.org/collection/NCLCollectionStore/:_Public/28/024/28024561.pdf
[86] Soh J-R, Schierle E, Yan DY, et al.Resonant x-ray scattering study of diffuse magnetic scattering from the topological semimetals $eucd_2as_2$ and $eucd_2sb_2$. Phys Rev B. 2020;102:014408. doi: 10.1103/PhysRevB.102.014408
[87] Stewart JR, Deen PP, Andersen KH, et al. Disordered materials studied using neutron polarization analysis on the multi-detector spectrometer, D7. J Appl Crystallogr. 2009;42:69–84. doi: 10.1107/S0021889808039162
[88] Gardner JS, Gingras MJP, Greedan JR. Magnetic pyrochlore oxides. Rev Mod Phys. 2010;82:53. doi: 10.1103/RevModPhys.82.53
[89] Binder K, Young AP. Spin glasses: experimental facts, theoretical concepts, and open questions. Rev Mod Phys. 1986;58:801. doi: 10.1103/RevModPhys.58.801
[90] Agrestini S, Fleck CL, Chapon LC, et al. Slow magnetic order-order transition in the spin chain antiferromagnet Ca3Co2O6. Phys Rev Lett. 2011;106:197204. doi: 10.1103/PhysRevLett.106.197204

[91] Shen L, Campillo E, Young E, et al. Magnetic microphase inhomogeneity as a thermodynamic precursor of ground-state phase separation in weakly coupled spin- 32 chains. Phys Rev B. 2021;103:134420. doi: 10.1103/PhysRevB.103.134420
[92] Pappas C, Ehlers G, Mezei F. Chapter 11 - neutron-spin-echo spectroscopy and magnetism. In: Chatterji T, editor. Neutron scattering from magnetic materials. Amsterdam: Elsevier Science; 2006. p. 521–542. doi: 10.1016/B978-044451050-1/50012-4
[93] Decker F-J, Bane KL, Colocho W, et al. Tunable x-ray free electron laser multi-pulses with nanosecond separation. Sci Rep. 2022;12:3253. doi: 10.1038/s41598-022-06754-y
[94] Fennell T, Bramwell ST, McMorrow DF, et al. Pinch points and kasteleyn transitions in kagome ice. Nat Phys. 2007;3:566–572. doi: 10.1038/nphys632
[95] Hoshino T, Fujinami S, Nakatani T, et al. Dynamical heterogeneity near glass transition temperature under shear conditions. Phys Rev Lett. 2020;124:118004. doi: 10.1103/PhysRevLett.124.118004
[96] Shen L, Esposito V, Burdet NG, etal. Interplay between atomic fluctuations and charge density waves in $la_{2-x}sr_xcuo_4$. Phys. Rev. B. 2023;108(20):L201111. doi: 10.1103/PhysRevB.108.L201111
[97] Song J, Patel, SK, Bhattacharya, R, et al. Direct measurement of temporal correlations above the spin-glass transition by coherent resonant magnetic x-ray spectroscopy. 2020. Available from: arXiv:2002.04259[cond-mat.supr-con]
[98] Blume M. Magnetic scattering of x rays (invited). J Appl Phys. 1985;57:3615–3618. doi: 10.1063/1.335023
[99] Hill JP, McMorrow DF. Resonant exchange scattering: polarization dependence and correlation function. Acta Crystallogr Sect A. 1996;52:236–244. doi: 10.1107/S0108767395012670
[100] Siegert A. MIT Radiation Laboratory Report, No. 465. 1943.
[101] Goodman J. Speckle phenomena in optics: theory and applications. Roberts & Company; 2007. Available from: https://books.google.com/books?id=TynXEcS0DncC
[102] Klose C, Büttner F, Hu W, et al. Photon correlation spectroscopy with heterodyne mixing based on soft x-ray magnetic circular dichroism. Phys Rev B. 2022;105:214425. doi: 10.1103/PhysRevB.105.214425
[103] Lhermitte JRM, Rogers MC, Manet S, et al. Velocity measurement by coherent x-ray heterodyning. Rev Sci Instrument. 2017;88:015112. doi: 10.1063/1.4974099
[104] Livet F, Bley F, Ehrburger-Dolle F, et al. Homodyne and heterodyne X-ray photon correlation spectroscopy: latex particles and elastomers. J Appl Crystallogr. 2007;40:s38–s42. doi: 10.1107/S0021889807003561
[105] Sun Y, Montana-Lopez J, Fuoss P, et al. Accurate contrast determination for x-ray speckle visibility spectroscopy. J Synchrotron Radiat. 2020;27:999–1007. doi: 10.1107/S1600577520006773
[106] Chitturi SR, Burdet NG, Nashed Y, et al. A machine learning photon detection algorithm for coherent x-ray ultrafast fluctuation analysis. Struct Dyn. 2022;9:054302. doi: 10.1063/4.0000161
[107] Hohenberg P, Kohn W. Inhomogeneous electron gas. Phys Rev. 1964;136:B864. doi: 10.1103/PhysRev.136.B864
[108] Kohn W, Sham LJ. Self-consistent equations including exchange and correlation effects. Phys Rev. 1965;140:A1133. doi: 10.1103/PhysRev.140.A1133
[109] Sun J, Ruzsinszky A, Perdew JP. Strongly constrained and appropriately normed semilocal density functional. Phys Rev Lett. 2015;115:036402. doi: 10.1103/PhysRevLett.115.036402

[110] Zhang Y, Lane C, Furness JW, et al. Competing stripe and magnetic phases in the cuprates from first principles. Proc Natl Acad Sci USA. 2020;117:68–72. doi: 10.1073/pnas.1910411116
[111] Moriya T. Anisotropic superexchange interaction and weak ferromagnetism. Phys Rev. 1960;120:91. doi: 10.1103/PhysRev.120.91
[112] Dzyaloshinsky I. A thermodynamic theory of "weak" ferromagnetism of antiferromagnetics. J Phys Chem Solids. 1958;4:241–255. doi: 10.1016/0022-3697(58)90076-3
[113] Skyrme THR. Selected papers, with commentary, of Tony Hilton Royle Skyrme, Brown GE, editor. Vol.3. Singapore: World Scientific; 1994.
[114] Müller GP, Hoffmann M, Dißelkamp C, et al. Spirit: multifunctional framework for atomistic spin simulations. Phys Rev B. 2019;99:224414. doi: 10.1103/PhysRevB.99.224414
[115] Mentink J, Tretyakov M, Fasolino A, et al. Stable and fast semi-implicit integration of the stochastic landau–lifshitz equation. J Phys Condens Matter. 2010;22:176001. doi: 10.1088/0953-8984/22/17/176001
[116] Behera AK, Chowdhury S, Das SR. Magnetic skyrmions in atomic thin cri3 monolayer. Appl Phys Lett. 2019;114:232402. doi: 10.1063/1.5096782
[117] Marzari N, Mostofi AA, Yates JR, et al. Maximally localized wannier functions: theory and applications. Rev Mod Phys. 2012;84:1419. doi: 10.1103/RevModPhys.84.1419
[118] Mostofi AA, Yates JR, Lee Y-S, et al. wannier90: a tool for obtaining maximally-localised wannier functions. Comput Phys Commun. 2008;178:685–699. doi: 10.1016/j.cpc.2007.11.016
[119] Korotin DM, Mazurenko V, Anisimov V, et al. Calculation of exchange constants of the heisenberg model in plane-wave-based methods using the green's function approach. Phys Rev B. 2015;91:224405. doi: 10.1103/PhysRevB.91.224405
[120] Plumley R, Mardanya S, Peng C, et al. 3D Heisenberg universality in the Van der waals antiferromagnet $NiPS_3$. 2023. Available from: arXiv:2310.07948
[121] Weiße A, Fehske H. Exact diagonalization techniques. Computational many-particle physics. Springer; 2008. p. 529–544.
[122] Hu W-J, Becca F, Parola A, et al. Direct evidence for a gapless z 2 spin liquid by frustrating néel antiferromagnetism. Phys Rev B. 2013;88:060402. doi: 10.1103/PhysRevB.88.060402
[123] Choo K, Neupert T, Carleo G. Two-dimensional frustrated J 1 – J 2 model studied with neural network quantum states. Phys Rev B. 2019;100:125124. doi: 10.1103/PhysRevB.100.125124
[124] Chen H, Hendry D, Weinberg P, et al. Systematic improvement of neural network quantum states using lanczos. Adv Neural Inf Process Syst. 2022;35:7490–7503.
[125] White SR. Density matrix formulation for quantum renormalization groups. Phys Rev Lett. 1992;69:2863–2866. doi: 10.1103/PhysRevLett.69.2863
[126] Loh Jr E, Gubernatis J, Scalettar R, et al. Sign problem in the numerical simulation of many-electron systems. Phys Rev B. 1990;41:9301. doi: 10.1103/PhysRevB.41.9301
[127] Troyer M, Wiese U-J. Computational complexity and fundamental limitations to fermionic quantum monte carlo simulations. Phys Rev Lett. 2005;94:170201. doi: 10.1103/PhysRevLett.94.170201
[128] Richter J, Schulenburg J. The spin-1/2 j1–j2 heisenberg antiferromagnet on the square lattice: exact diagonalization for n= 40 spins. Eur Phys J B. 2010;73:117–124. doi: 10.1140/epjb/e2009-00400-4
[129] McCulloch IP. From density-matrix renormalization group to matrix product states. J Stat Mech Theory Experiment. 2007;2007:P10014. doi: 10.1088/1742-5468/2007/10/P10014

[130] Pirvu B, Murg V, Cirac JI, et al. Matrix product operator representations. New J Phys. 2010;12:025012. doi: 10.1088/1367-2630/12/2/025012
[131] Schollwöck U. The density-matrix renormalization group in the age of matrix product states. Ann Phys. 2011;326:96–192. doi: 10.1016/j.aop.2010.09.012
[132] White SR. Density matrix renormalization group algorithms with a single center site. Phys Rev B. 2005;72:180403. doi: 10.1103/PhysRevB.72.180403
[133] Dolfi M, Bauer B, Troyer M, et al. Multigrid algorithms for tensor network states. Phys Rev Lett. 2012;109:020604. doi: 10.1103/PhysRevLett.109.020604
[134] Stoudenmire EM, White SR. Real-space parallel density matrix renormalization group. Phys Rev B. 2013;87:155137. doi: 10.1103/PhysRevB.87.155137
[135] Kühner TD, White SR. Dynamical correlation functions using the density matrix renormalization group. Phys Rev B. 1999;60:335–343. doi: 10.1103/PhysRevB.60.335
[136] Cazalilla MA, Marston JB. Time-dependent density-matrix renormalization group: a systematic method for the study of quantum many-body out-of-equilibrium systems. Phys Rev Lett. 2002;88:256403. doi: 10.1103/PhysRevLett.88.256403
[137] Burdet NG, Esposito V, Seaberg M, et al. Absolute contrast estimation for soft x-ray photon fluctuation spectroscopy using a variational droplet model. Sci Rep. 2021;11:19455. doi: 10.1038/s41598-021-98774-3
[138] Hruszkewycz SO, Sutton M, Fuoss PH, et al. High contrast x-ray speckle from atomic-scale order in liquids and glasses. Phys Rev Lett. 2012;109:185502. doi: 10.1103/PhysRevLett.109.185502
[139] Sun Y, Decker F-J, Turner J, et al. Pulse intensity characterization of the LCLS nanosecond double-bunch mode of operation. J Synchrotron Radiat. 2018;25:642–649. doi: 10.1107/S160057751800348X
[140] Samarakoon AM, Barros K, Li YW, et al. Machine-learning-assisted insight into spin ice $Dy_2Ti_2O_7$. Nat Commun. 2020;11:892. doi: 10.1038/s41467-020-14660-y
[141] Doucet M, Samarakoon AM, Do C, et al. Machine learning for neutron scattering at ORNL. Mach Learn Sci Technol. 2020;2:023001. doi: 10.1088/2632-2153/abcf88
[142] Samarakoon A, Tennant DA, Ye F, et al. Integration of machine learning with neutron scattering for the hamiltonian tuning of spin ice under pressure. Commun Mater. 2022;**3**:84. doi: 10.1038/s43246-022-00306-7
[143] Samarakoon AM, Laurell P, Balz C, et al. Extraction of interaction parameters for α – RuCl 3 from neutron data using machine learning. Phys Rev Res. 2022;4:L022061. doi: 10.1103/PhysRevResearch.4.L022061
[144] Chitturi SR, Ji Z, Petsch AN, et al. Capturing dynamical correlations using implicit neural representations. Nat Commun. 2023;14:5852. doi: 10.1038/s41467-023-41378-4
[145] Petsch AN, Headings NS, Prabhakaran D, et al. High-energy spin waves in the spin-1 square-lattice antiferromagnet La 2 NiO 4. Phys Rev Res. 2023;5. doi: 10.1103/PhysRevResearch.5.033113
[146] Butler KT, Le MD, Thiyagalingam J, et al. Interpretable, calibrated neural networks for analysis and understanding of inelastic neutron scattering data. J Phys Condens Matter. 2021;33:194006. doi: 10.1088/1361-648X/abea1c
[147] Han J, Shoeiby M, Petersson L, et al. Dual contrastive learning for unsupervised image-to-image translation. In: Proceedings of the IEEE/CVF conference on computer vision and pattern recognition; 2021. p. 746–755. Available from: https://openaccess.thecvf.com/content/CVPR2021W/NTIRE/papers/Han:_Dual:_Contrastive:_Learning:_for:_Unsupervised:_Image-to-Image:_Translation:_CVPRW:_2021:_paper.pdf

[148] Anker AS, Butler KT, Le MD, et al. Using generative adversarial networks to match experimental and simulated inelastic neutron scattering data. Digit Discov. 2023;2:578–590. doi: 10.1039/D2DD00147K
[149] Granade CE, Ferrie C, Wiebe N, et al. Robust online hamiltonian learning. New J Phys. 2012;14:103013. doi: 10.1088/1367-2630/14/10/103013
[150] Huan X, Marzouk YM. Simulation-based optimal bayesian experimental design for nonlinear systems. J Comput Phys. 2013;232:288–317. doi: 10.1016/j.jcp.2012.08.013
[151] McMichael RD, Blakley SM. Simplified algorithms for adaptive experiment design in parameter estimation. Phys Rev Appl. 2022;18:054001. doi: 10.1103/PhysRevApplied.18.054001
[152] Dushenko S, Ambal K, McMichael RD. Sequential bayesian experiment design for optically detected magnetic resonance of nitrogen-vacancy centers. Phys Rev Appl. 2020;14:054036. doi: 10.1103/PhysRevApplied.14.054036
[153] McMichael RD, Dushenko S, Blakley SM. Sequential bayesian experiment design for adaptive ramsey sequence measurements. J Appl Phys. 2021;130. doi: 10.1063/5.0055630
[154] Caouette-Mansour M, Solyom A, Ruffolo B, et al. Robust spin relaxometry with fast adaptive bayesian estimation. Phys Rev Appl. 2022;17:064031. doi: 10.1103/PhysRevApplied.17.064031
[155] Chen Z, Peng C, Petsch AN, et al. Bayesian experimental design and parameter estimation for ultrafast spin dynamics. Mach Learn Sci Technol. 2023;4:045056. doi: 10.1088/2632-2153/ad113a
[156] Lutman AA, Maxwell TJ, MacArthur JP, et al. Fresh-slice multicolour x-ray free-electron lasers. Nat Phot. 2016;10:745. doi: 10.1038/nphoton.2016.201
[157] Razzoli E, Ueda H, Paris E, et al. Ultrafast dynamics in quantum matter at swissfel: capabilities of furka endstation. X-Ray Free-Electron Lasers Adv Source Devel Instrum VI. 2023;12581 SPIE, 68–70.
[158] Mankowsky R, Sander M, Zerdane S, et al. New insights into correlated materials in the time domain—combining far-infrared excitation with x-ray probes at cryogenic temperatures. J Phys Condens Matter. 2021;33:374001. doi: 10.1088/1361-648X/ac08b5
[159] Ueda H, Mankowsky R, Paris E, et al. Non-equilibrium dynamics of spin-lattice coupling. Nat Commun. 2023;14:7778. doi: 10.1038/s41467-023-43581-9
[160] Fechner M, Först M, Orenstein G, et al. Quenched lattice fluctuations in optically driven srtio3. Nat Mater. 2024;23:363–368. doi: 10.1038/s41563-023-01791-y
[161] Tschentscher T, Bressler C, Grünert J, et al. Photon beam transport and scientific instruments at the european xfel. Appl Sci. 2017;7:592. doi: 10.3390/app7060592
[162] Kunnus K, Rajkovic I, Schreck S, et al. A setup for resonant inelastic soft x-ray scattering on liquids at free electron laser light sources. Rev Sci Instrum. 2012;83:123109–123109–8. doi: 10.1063/1.4772685
[163] Wernet P, Kunnus K, Josefsson I, et al. Orbital-specific mapping of the ligand exchange dynamics of Fe(CO)5 in solution. Nature. 2015;520:78–81. doi: 10.1038/nature14296
[164] Kimura T, Hatsuda K, Ueno Y, et al. Charge-orbital ordering and ferromagnetic chains in single-layered manganite crystals. Phys Rev B. 2001;65:020407. doi: 10.1103/PhysRevB.65.020407
[165] Fujioka J, Ida Y, Takahashi Y, et al. Optical investigation of the collective dynamics of charge-orbital density waves in layered manganites. Phys Rev B. 2010;82:140409. doi: 10.1103/PhysRevB.82.140409
[166] Minitti MP, Robinson JS, Coffee RN, et al. Optical laser systems at the linac coherent light source. J Synchrotron RAD. 2015;22:526–531. doi: 10.1107/S1600577515006244

[167] Schneider A, Neis M, Stillhart M, et al. Generation of terahertz pulses through optical rectification in organic dast crystals: theory and experiment. J Opt Soc Am B. 2006;23:1822–1835. doi: 10.1364/JOSAB.23.001822
[168] Vicario C, Jazbinsek M, Ovchinnikov AV, et al. High efficiency thz generation in dstms, dast and oh1 pumped by cr: forsterite laser. Opt Express. 2015;23:4573–4580. doi: 10.1364/OE.23.004573
[169] Doering D, Chuang YD, Andresen N, et al. Development of a compact fast ccd camera and resonant soft x-ray scattering endstation for time-resolved pump-probe experiments. Rev Sci Instrum. 2011;82:073303–073303–8. doi: 10.1063/1.3609862
[170] Chesnel K, Turner JJ, Pfeifer M, et al. Probing complex materials with coherent soft x-rays. Appl Phys A. 2008;92:431–437. doi: 10.1007/s00339-008-4558-3
[171] Heimann P, Krupin O, Schlotter WF, et al. Linac coherent light source soft x-ray materials science instrument optical design and monochromator commissioning. Rev Sci Instrum. 2011;82:093104–093104–8. doi: 10.1063/1.3633947
[172] Tiedtke K, Sorokin AA, Jastrow U, et al. Absolute pulse energy measurements of soft x-rays at the linac coherent light source. Opt Express. 2014;22:21214–21226. doi: 10.1364/OE.22.021214
[173] Chalupsky J, Bohacek P, Hajkova V, et al. Comparing different approaches to characterization of focused x-ray laser beams. Nucl Instrum Methods Phys Res A. 2011;631:130–133. doi: 10.1016/j.nima.2010.12.040
[174] Chalupský J, Boháček P, Burian T, et al. Imprinting a focused x-ray laser beam to measure its full spatial characteristics. Phys Rev Appl. 2015;4:014004. doi: 10.1103/PhysRevApplied.4.014004
[175] Moeller S, Brown G, Dakovski G, et al. Pulse energy measurement at the sxr instrument. J Synchrotron RAD. 2015;22:606–611. doi: 10.1107/S1600577515006098

Appendix A. Experimental methods

1 Single crystal $Nd_{1-x}Sr_{1+x}MnO_4$ for x = 2/3

The experiment discussed in Sec. 2.1 on $Nd_{1-x}Sr_{1+x}MnO_4$ for $x = 2/3$ was a single crystal grown by the floating-zone method [164] and polished along the (110) direction. Complementary measurements of optical conductivity [165], 800 nm pump-probe measurements with soft x-ray resonant probe [60], and time-resolved optical reflectivity measurements [60] have previously been carried out. A high-power Ti:sapphire-based laser (1.55 eV) with a 50-fs pulse duration and 120-Hz repetition rate which was split and cross-polarized for the pump pulses, which gives a temporal resolution of about 75 fs [166]. THz generation was produced through non-linear rectification using an ionic organic crystal 4-N-methylstilbazolium tosylate (DAST) [167] to generate field strengths in excess of 300 kV/cm [168] (See Figure 2a). By cooling the sample with a liquid He cryostat in UHV [64, 169], the crystal could be studied below the Néel temperature of 90 K [60].

2 Multilayered FeGd

The experiments on multilayered FeGd described in Sec. 2.2 were taken using the XPFS prototype instrument [72] in a forward scattering geometry of the new chemRIXS endstation designed for the next-generation X-FEL LCLS-II. The image was collected at the L_3–edge resonance for Fe of ∼eV by tuning the X-FEL electon energy ahd following it with the monochromator.

The sample measured is a multilayer with 100 repetitions of alternating Fe (0.34 nm) and Gd (0.4 nm) layers grown by dc magnetron sputtering. This system can be adjusted in total thickness to optimize the scattering intensity and the alloy composition can be tuned to produce different phases. They were deposited on 50 nm Si_3N_4 membranes and were measured in a forward scattering geometry. The samples were precharacterized at a coherent soft x-ray beam line at the Advanced Light Source [170].

3 Thin film CuMn

The experiments on thin film CuMn in Sec. 2.3 were taken using the XPFS prototype instrument [72] in a forward scattering geometry of the SXR instrument at the LCLS [63, 65]. The image was collected at the L_3–edge resonance for Mn of ∼eV [171]. The bandwidth was about ∼eV [172] with a large spot size of 150 μm to avoid beam damage [173, 174]. The detector was placed 1.016 m away from the sample. Different thicknesses of aluminum filters were also used to vary the pulse energy, which was on about the scale of 1×10^{-4}mJ per pulse on average after the monochromator [175]. The pulse duration was about 100fs and was delivered at 120Hz repetition rate. The image in Figure 4c

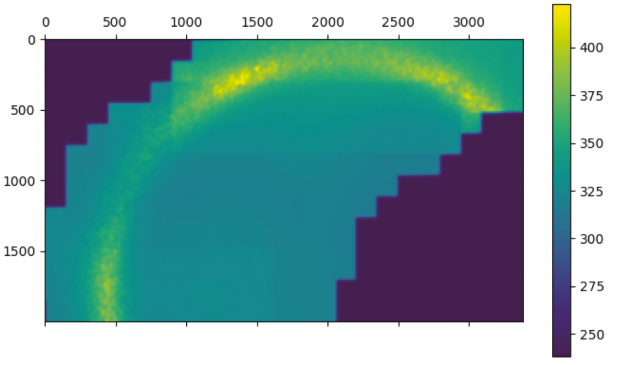

Figure A1. This is the first result given by the XPFS setup installed at the chemRIXS instrument. By stitching together many images, the phase of the FeGd system could be identified to be at the stripe-skrymion phase boundary.

shows spin-glass speckle using a 500×500 pixel image. The full detector is off-center of the peak to capture optimal diffuse scattering.

Appendix B. First results from XPFS at the chemRIXS instrument

This appendix describes the first results obtained from the XPFS prototype instrument implemented at the chemRIXS beamline of the LCLS-II. The chemRIXS instrument was designed for ultrafast spectroscopy of a liquid chemistry environment, and hence provided no opportunities for an experiment in magnetism (see Section 5.3.2) which motivated the design and realization of this system.

In order to compile the complete magnetic scattering distribution, the detector must span the full regions of reciprocal space in order to identify the phase. Because this system can have 2-fold symmetry, 6-fold symmetry, or a full continuous disordered ring, a large region of reciprocal space must be explored. We performed the stitching using a pairwise phase correlation in sequence. The position of the detector was not encoded, so this was accomplished by first finding the relative shift between detector images, then summing images with the same position. The next step is that this is normalized by a weighting matrix calculated from the overlapping areas. The image presented here was the result of stitching 643 images, which was enough to conclude the phase of the sample for the measurement.